

Decoupling Exploration and Policy Optimization: Uncertainty Guided Tree Search for Hard Exploration

Zakaria Mhammedi
Google Research, NYC
mhammedi@google.com

James Cohan
Google Research, NYC
jamesfcohan@google.com

May 14, 2026

Abstract

The process of discovery requires active exploration—the act of collecting new and informative data. However, efficient autonomous exploration remains a major unsolved problem. The dominant paradigm addresses this challenge by using Reinforcement Learning (RL) to train agents with intrinsic motivation, maximizing a composite objective of extrinsic and intrinsic rewards. We suggest that this approach incurs unnecessary overhead: while policy optimization is necessary for precise task execution, employing such machinery solely to expand state coverage may be inefficient. In this paper, we propose a new approach that explicitly decouples exploration from policy optimization and bypasses RL entirely during the exploration phase. Our method uses a tree-search strategy inspired by the Go-With-The-Winner algorithm, paired with a measure of uncertainty to systematically drive exploration. By removing the overhead of policy optimization, our approach explores an order of magnitude more efficiently than standard intrinsic motivation baselines on hard exploration benchmarks. Further, we demonstrate that the trajectories discovered during exploration can be distilled into deployable policies using existing supervised backward learning algorithms, achieving state-of-the-art performance by a wide margin on *Montezuma’s Revenge*, *Pitfall!*, and *Venture* without relying on domain-specific knowledge. Finally, we demonstrate the generality of our framework in high-dimensional continuous action spaces by solving the MuJoCo Adroit dexterous manipulation and AntMaze tasks in a *sparse-reward* setting, directly from image observations and without expert demonstrations or offline datasets. To the best of our knowledge, this has not been achieved before for the Adroit tasks.

1 Introduction

Reinforcement learning (RL) is a cornerstone of modern artificial intelligence, enabling breakthroughs in complex autonomous systems and, more recently, the post-training and alignment of Large Language Models (LLMs) (Mnih et al., 2015; Silver et al., 2016, 2018; Ouyang et al., 2022; Rafailov et al., 2023). However, these successes often rely on rich feedback, such as expert demonstrations in robotics or preference labels in language model alignment (Christiano et al., 2017; Hester et al., 2018; Brohan et al., 2022). In the settings we study—where rewards are sparse or the goal is to surpass human performance—agents must go beyond imitation and autonomously discover novel behavior.

This requires *active exploration*: an algorithmic process that deliberately collects informative experience (Shyam et al., 2019; Sekar et al., 2020; Eysenbach et al., 2018). In the hardest cases, this amounts to “finding a needle in a haystack,” where a single rare trajectory is the key that unlocks learning. In structured settings like two-player games, self-play facilitates exploration (Silver et al., 2016). The adversarial dynamic ensures that novel strategies are always within reach of each agent’s current policy. Outside self-play, driving exploration is significantly harder. Even in simple 2D environments, current methods often fail to explore efficiently without domain engineering; *Montezuma’s Revenge* and *Pitfall!* remain standard benchmarks that stress-test systematic exploration (Ecoffet et al., 2019; Badia et al., 2020a,b; Guo et al., 2022). These persistent failures highlight that systematic exploration in sparse-reward settings remains poorly understood.

Unlocking efficient exploration would have impact well beyond games, enabling autonomous discovery in various scientific domains.

Historically, the primary approach to exploration relies on training agents with *intrinsic motivation* (Schmidhuber, 1991; Oudeyer et al., 2007; Barto, 2012; Houthoofd et al., 2016; Stadie et al., 2015). In this paradigm, the agent is trained to maximize a combined objective: the task reward plus an auxiliary signal designed so that maximizing it encourages the agent to visit novel states. In high-dimensional spaces, this auxiliary signal, commonly referred to as *intrinsic reward* or *bonus*, typically consists of a proxy for “visitation frequency,” such as the error of Random Network Distillation (RND) or the prediction error of a dynamics model (Burda et al., 2018; Pathak et al., 2017, 2019). While accurate uncertainty estimation is crucial, we argue that driving exploration by maximizing these signals via RL incurs unnecessary complexity; iteratively updating a policy to reach novel states is inherently sample-inefficient, as it requires constantly tracking a non-stationary intrinsic reward signal.

Contributions.

- We propose a new paradigm for autonomous exploration in sparse-reward settings that bypasses intrinsic-reward policy optimization. Our framework pairs a tree-search strategy, inspired by the Go-With-The-Winner (GWTW) algorithm (Aldous and Vazirani, 1994), with epistemic uncertainty (a measure of the agent’s uncertainty about a state given limited exposure to it) (Depeweg et al., 2018) to drive exploration; the approach is modular and agnostic to the specific uncertainty metric. The method relies on the ability to *reset* the environment to previously visited states in order to redistribute computational effort toward the most promising frontiers. By replacing intrinsic-reward policy optimization with uncertainty-guided tree search, our method discovers high-reward trajectories using an order of magnitude fewer environment interactions than standard intrinsic motivation baselines on hard-exploration benchmarks.
- We show that supervised backward learning algorithms (e.g., Salimans and Chen (2018)) can distill the generated trajectories into deployable, high-scoring policies. In particular, we achieve state-of-the-art results by a wide margin on *Montezuma’s Revenge*, *Pitfall!*, and *Venture* when not relying on domain-specific knowledge.
- We demonstrate the generality of our framework by applying it to high-dimensional continuous action spaces, solving the MuJoCo Adroit dexterous manipulation and AntMaze navigation tasks from pixel observations in a *sparse-reward* setting without relying on expert demonstrations or offline datasets. To the best of our knowledge, this has not been previously achieved for the Adroit tasks. In both cases, the final distilled policies operate directly from image observations, without accessing privileged state information.

Outline. The remainder of this paper is organized as follows. [Section 2](#) presents the related work and contextualizes our approach within the literature on exploration. [Section 3](#) formalizes the problem setting and introduces core components, including the uncertainty estimator and the reset mechanism. [Section 4](#) details our uncertainty-driven tree-search algorithm for exploration, GO-WITH-UNCERTAINTY (GOWU). Finally, [Section 5](#) evaluates the method on hard-exploration Atari games and challenging MuJoCo continuous-control tasks, showing efficient exploration and successful policy distillation across all environments.

2 Related Work

Efficient exploration remains a central challenge in reinforcement learning. Below we situate our approach within the broader landscape of exploration methods.

Intrinsic motivation and latent predictive models. A dominant approach to exploration in deep RL is to train a policy to maximize an intrinsic motivation signal that encourages the agent to visit novel states (Stadie et al., 2015; Bellemare et al., 2016; Pathak et al., 2019; Badia et al., 2020a). In high-dimensional settings, these signals are often defined using proxies for novelty such as prediction error (Pathak et al., 2017), pseudo-counts (Bellemare et al., 2016), Random Network Distillation (Burda et al., 2018), or information gain over a learned dynamics model (Houthoofd et al., 2016). Recent methods such as BYOL-Explore (Guo et al., 2022) continue this line by defining the intrinsic signal through the error in predicting future latent representations, an elegant way to measure novelty in high-dimensional observations. BYOL-Hindsight (Jarrett et al., 2023) extends this approach to better handle stochastic environments. These methods are

among the strongest intrinsic-motivation baselines on hard-exploration benchmarks, yet even they remain limited on the hardest sparse-reward problems (such as *Montezuma’s Revenge* and *Pitfall!*), especially once stochasticity is introduced. This supports our view that maximizing intrinsic motivation signals through standard policy optimization may be fundamentally inefficient for hard exploration.

Separating exploration from exploitation. Another line of work separates exploration and downstream task optimization into distinct phases. In the empirical literature, this perspective appears in reward-free or unsupervised RL setups such as URLB (Laskin et al., 2021), where an agent first performs task-agnostic pre-training and is only later adapted to downstream rewards. Methods such as APT (Liu and Abbeel, 2021) and Plan2Explore (Sekar et al., 2020) allocate this pre-training phase to broad state discovery using intrinsic objectives such as state coverage or model uncertainty, while skill-discovery methods such as variational intrinsic control (Mohamed and Jimenez Rezende, 2015) and DIAYN (Eysenbach et al., 2018) learn diverse behaviors before task rewards are introduced. This perspective also appears in the theoretical literature. A canonical early example is E^3 (Kearns and Singh, 2002), which formalizes an explicit explore-or-exploit strategy. The reward-free exploration framework of Jin et al. (2020) goes further by showing that a pure exploration phase can suffice for efficient downstream planning in tabular MDPs. Subsequent work studies related ideas in rich-observation settings with discrete (Misra et al., 2020; Mhammedi et al., 2023b) and low-rank transition structure (Mhammedi et al., 2023a).

Exploration without policy optimization. While the approaches above separate exploration from exploitation, the exploration phase itself still relies on policy optimization to maximize an intrinsic objective. Our approach departs from this by decoupling exploration from policy optimization entirely. To our knowledge, among methods that go beyond tabular settings, the only other approach that does this is Go-Explore (Ecoffet et al., 2019, 2021). Both methods treat exploration as a search problem rather than as the optimization of an intrinsic reward, but the search mechanisms are fundamentally different; instead of maintaining an archive over discretized cells and repeatedly returning to archived states, we use a particle-based tree-search procedure guided by an epistemic uncertainty signal. Crucially, our method does not rely on hand-designed observation discretization or deterministic dynamics (Latent Go-Explore bypasses both but has other limitations; see Appendix H), making it more naturally suited to high-dimensional and stochastic environments. Despite these differences, both approaches share a common role: generating successful trajectories that can later be distilled into deployable policies through backward learning (Salimans and Chen, 2018; Ecoffet et al., 2019).

Leveraging resets as a computational primitive. Both GO-EXPLORE and our approach rely on a shared computational primitive: the ability to reset the environment to a previously visited state. This capability is also central to search-based methods such as Monte Carlo Tree Search (MCTS), which repeatedly branch from simulator states during planning (Kocsis and Szepesvári, 2006; Coulom, 2006). While arbitrary resets are often impractical on physical systems (Eysenbach et al., 2017; Gupta et al., 2021), they are readily available in simulation, where much of modern RL training already takes place (Zhao et al., 2020; Aljalbout et al., 2025). Recent theoretical work shows that local simulator access enables efficient learning in settings where standard online RL is provably inefficient (Li et al., 2021; Yin et al., 2023; Mhammedi et al., 2024). Our work treats resets as a training-time tool for exploration: they allow the algorithm to repeatedly redirect computation toward promising frontier states, without requiring simulator access at inference time.

Relationship to MCTS. Although GowU and MCTS both build search trees using simulator access, they differ substantially in both purpose and mechanism. MCTS is a planning algorithm that learns a value function during training and uses it at inference time to guide a search tree for action selection (Kocsis and Szepesvári, 2006; Coulom, 2006). GowU serves a fundamentally different purpose: it is a purely training-time procedure that discovers successful trajectories but produces no policy or value function. The actions taken during search are discarded; only the discovered state sequences are retained, which a second phase then uses to learn a policy. Beyond this difference in purpose, the search procedures themselves are fundamentally different. GowU is a population-based algorithm inspired by the Go-With-The-Winner principle (Aldous and Vazirani, 1994): a population of particles evolves concurrently through the state space, with explicit cloning, pruning, and winner-selection operations that have no analogue in MCTS (see Appendix H for further differences).

Evolutionary and population-based methods. GowU’s population-based nature also connects it to

evolutionary methods, which drive exploration by evolving diverse populations of policies. However, unlike GowU, which searches directly in state space, these methods operate in the parameter space of a policy, generating diversity by perturbing model parameters (see [Appendix H](#) for more details).

3 Preliminaries

We consider the problem of exploration in a stochastic episodic Markov Decision Process (MDP) defined by the tuple $\mathcal{M} = (\mathcal{X}, \mathcal{A}, P, R)$. Here, \mathcal{X} and \mathcal{A} are potentially large or infinite state and action spaces, respectively; $P : \mathcal{X} \times \mathcal{A} \rightarrow \Delta(\mathcal{X})$ is the transition function, and $R : \mathcal{X} \times \mathcal{A} \rightarrow \mathbb{R}$ is a deterministic reward function. The rest of this section introduces the building blocks of our approach.

Survival and failure. Episodic MDPs define termination conditions that mark the end of a trajectory. For instance, in games like Atari, an episode typically ends after *all* lives are lost. Our framework allows for distinguishing between this standard termination and a stricter notion of *failure* we use for early episode truncation. In the Atari context, for example, we may treat the loss of a single life as a failure event; similarly, in continuous control, a state from which further progress is impossible (e.g., a quadruped flipping upside down in the AntMaze environment) can be treated as a failure, even if the environment does not formally terminate the episode. We demonstrate that using this flexibility can significantly improve exploration efficiency.

To formalize this, we partition the state space into viable states (ALIVE) and failure states (DEAD). We further define DOOM states, $\mathcal{X}_{\text{DOOM}} \subset \text{ALIVE}$, as viable states from which failure is inevitable regardless of the policy. Our approach is designed for settings where progress—accumulating rewards or task completion—remains feasible from any non-DOOM viable state.

Go-With-The-Winner (GWTW). To discover high-reward trajectories efficiently, our method builds on the Go-With-The-Winner (GWTW) principle ([Aldous and Vazirani, 1994](#)). Originally proposed for randomized search and sampling, GWTW is especially effective at finding deep nodes in imbalanced trees—a task where naive approaches like Depth-First or Breadth-First search can be computationally inefficient (see [Appendix K](#) for a concrete example). The algorithm operates by maintaining a population of N particles starting at the root. At each step, every particle advances one level by following a random edge. Crucially, particles that reach a leaf are pruned and replaced by clones of particles that reached non-leaf nodes, designated as “winners.” Theoretical guarantees for reaching a target depth in GWTW worsen gracefully with a measure of tree imbalance ([Aldous and Vazirani, 1994](#)). Our approach builds on this principle by viewing exploration in an MDP as a search for “deep” nodes, where depth is characterized by high cumulative reward and epistemic uncertainty.

To adapt GWTW for exploration, we map “leaves” to DEAD states and redefine “winners” as states combining high accumulated reward and (epistemic) uncertainty.

Uncertainty oracle. Our winner criterion depends on a measure of epistemic uncertainty—the lack of knowledge resulting from limited data, as opposed to the inherent stochasticity of the environment ([Osband et al., 2018](#); [Kendall and Gal, 2017](#); [Burda et al., 2018](#)). We assume access to an uncertainty estimator, U , that assigns a scalar score to each state and updates online: as a state is visited more, its uncertainty decreases. The framework is agnostic to the choice of U ; in our experiments, we use RND prediction error as a proxy ([Burda et al., 2018](#)).

Reset oracle. To enable cloning (as in GWTW), we require overwriting one particle’s state with another’s via a reset primitive (see [Appendix C](#) for implementation details).

Backward algorithm. Our new exploration algorithm does not produce a policy; it produces trajectories—sequences of environment checkpoints recording states visited by the most successful particles. These trajectories can be used in a second phase to learn deployable policies. Although the trajectories may contain redundancies or suboptimal loops, they serve as self-generated demonstrations for backward learning algorithms ([Salimans and Chen, 2018](#); [Ecoffet et al., 2019](#)). This class of algorithms begins training near the end of a demonstration and progressively moves the starting state backward as the agent masters each suffix segment, creating a natural curriculum that significantly simplifies the reinforcement learning problem. In our

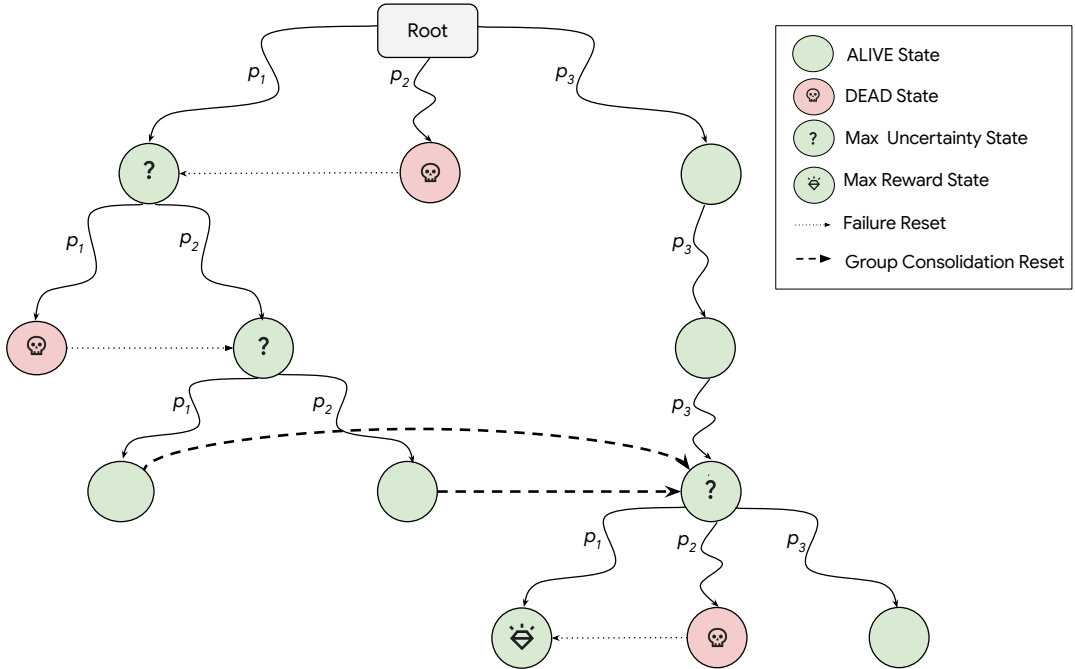


Figure 1: Schematic overview of GowU with a single group of particles. The algorithm maintains a population of particles (p_1, p_2, p_3) that explore the state space via multi-step rollouts. During an outer step, if a particle reaches a DEAD state (e.g., p_2 on level one), it is pruned and its state is reset via a *Reset* to the winner—the ALIVE node maximizing accumulated reward, with epistemic uncertainty used as a tie-breaker. After K outer steps, a *Group Consolidation Reset* syncs all particles, including ALIVE particles, to the current winner.

experiments, we use this framework to obtain high-scoring policies across all environments (see [Appendix B](#) for full implementation details).

4 Method: Uncertainty-Guided Exploration

Building on the primitives in [Section 3](#), we propose GO-WITH-UNCERTAINTY (GOWU), a tree-search method decoupling exploration from policy optimization. Our approach adapts the GWTW principle by maintaining a population of particles that explore the state space in parallel. At fixed intervals, the algorithm identifies “winners”—those in states with high cumulative reward and epistemic uncertainty. Using the reset oracle, it redistributes computational effort by cloning winners and removing DEAD particles.

We first describe the state-lineage tree, which tracks particle history and enables population management. We then detail particle evolution and the winner selection scoring function, referencing the pseudo-algorithms [Algorithms 1](#) and [2](#) along the way.

4.1 The State Lineage Tree

To manage populations, GOWU maintains a global *state-lineage tree*. Each node in this tree represents a valid, checkpointed state of the environment. Formally, a tree node v is a tuple (s_v, R_v, u_v) , where s_v is the compact state representation (e.g., simulator snapshot); R_v is the cumulative extrinsic reward achieved by the agent up to state s_v ; and u_v is a pointer to the PARENT node.

This structure allows the algorithm to track the history of every particle. To manage memory, nodes are pruned when they are no longer occupied by an active particle or referenced by any descendant. This ensures that the storage requirements scale only with the set of active lineages.

4.2 Particle Evolution

We now describe the search procedure, which implements our adaptation of GWTW to drive exploration using a group of N particles (e.g., $N = 32$ for some of our experiments). The search proceeds in discrete iterations. [Algorithm 1](#) details the execution of a single iteration, which consists of a sequence of K OUTER STEPS, followed by a synchronization phase, where K is sampled uniformly from $[K_{\min}, K_{\max}]$ at the start of each iteration.

Evolutionary rollout. During an outer step, every ALIVE particle interacts with its own instance of the environment for a random number of simulation steps (INNER STEPS) sampled independently for each particle from the range $[T_{\min}, T_{\max}]$ (see [Algorithm 1, Line 4](#)). Our framework is agnostic to the mechanism each particle uses to select actions; in practice, we employ random policies as described in [Section 4.4](#). During the INNER STEPS, the uncertainty estimator U may update based on newly collected observations. If a particle receives a positive reward, the rollout is terminated immediately ([Algorithm 1, Line 8](#)); this secures the reward for the subsequent winner selection, as further steps may lead to a DEAD state. If a particle completes the rollout without entering a DEAD state, the algorithm creates a new child node in the lineage tree ([Algorithm 1, Line 11](#)). The rollout length range controls a key trade-off: overly short rollouts limit state diversity, while overly long ones increase the frequency of DEAD states. (In our experiments, T_{\min} and T_{\max} are set between 3 and 20.)

Failure recovery via rollback. If the entire population enters a DEAD state during a rollout, the algorithm performs a collective ROLLBACK. Every particle traverses the lineage tree via parent pointers u_v to a randomly selected ancestor between k_{\min} and k_{\max} generations prior ([Algorithm 1, Line 17](#)). This restores the particles to valid antecedent states, allowing exploration of alternative trajectories around, for example, obstacles. A sufficiently large k_{\max} allows particles to escape *doom states* (e.g., irreversible falls), while a low k_{\min} maintains proximity to difficult obstacles, enabling alternative trajectory attempts ($k_{\min}, k_{\max} \in [1, 20]$ in our experiments).

Winner selection and particle redistribution. When at least one particle survives the INNER STEPS rollout, the algorithm redistributes computational effort by identifying “winners.”

1. *Winner selection:* The algorithm identifies the ALIVE particles with the maximum accumulated reward. Among these, it selects the particle with the highest uncertainty $U(s)$ ([Algorithm 1, Line 20](#)). This prioritizes high-value, under-explored states; in environments with sparse rewards (like the ones in our experiments), uncertainty is often the primary criterion for selection.
2. *Pruning:* All DEAD particles are immediately reset to the winner’s state ([Algorithm 1, Line 23](#)). This prunes failed branches and redirects those resources to the current frontier. Non-winner ALIVE particles continue independent trajectories to maintain local diversity.

Group consolidation. At the conclusion of the K OUTER STEPS, the algorithm performs an additional synchronization to consolidate progress. We identify a single group winner based on accumulated reward and uncertainty as in [Item 1](#). Unlike the mid-iteration redistribution, where only DEAD particles are reset, this step collapses the entire group to the winner’s state ([Algorithm 1, Line 30](#)), ensuring the next iteration begins from the most promising frontier discovered so far.

4.3 Parallel Groups and Population Synchronization

To diversify the search and accelerate discovery, GOWU runs M groups in parallel; see [Algorithm 2](#) (e.g., $M = 4$ for our Atari experiments). While these groups may execute rollouts independently, our framework allows the groups to share a centralized uncertainty estimator. This enables implicit coordination: updates from one group discourage others from revisiting the same states, pushing the collective population toward globally novel regions. To further prevent groups from stagnating in explored regions, the algorithm employs a global synchronization mechanism at the start of each iteration. We identify a single “global winner” across

Algorithm 1 EVOLVEGROUP

```
input: Population  $P = \{p_1, \dots, p_N\}$ , lineage tree  $\mathcal{T}$ , uncertainty  $U$ 
params: OUTER STEPS, INNER STEPS, and ROLLBACK ranges:  $[K_{\min}, K_{\max}]$ ,  $[T_{\min}, T_{\max}]$ ,  $[k_{\min}, k_{\max}]$ 

1: Sample OUTER STEPS  $K \sim \text{Unif}(K_{\min}, K_{\max})$ 
2: for  $k = 1, \dots, K$  do
3:   for each particle  $p_i \in P$  do
4:     Sample INNER STEPS  $T_i \sim \text{Unif}(T_{\min}, T_{\max})$ 
5:     /* Rollout particle and update uncertainty */
6:     for  $t = 1, \dots, T_i$  do
7:        $U \leftarrow p_i.\text{STEP}(1, U)$  // Execute one step
8:       if  $p_i$  is DEAD or  $p_i.R$  increased then break // Halting on reward does not kill the particle
9:     end for
10:    if  $p_i$  is ALIVE then
11:       $\mathcal{T}.\text{ADDCHILD}(p_i)$  // Expand tree for surviving particles
12:    end if
13:  end for
14:  if All  $p_i \in P$  are DEAD then
15:    /* Failure recovery via rollback */
16:     $v_{i,\text{ANC}} \leftarrow p_i.\text{GETANCESTOR}(k_{\min}, k_{\max}), \forall i$  // Pick  $k_i$ th ancestor of  $p_i$  with  $k_i \sim \text{Unif}(k_{\min}, k_{\max}), \forall i$ 
17:     $P \leftarrow \{\text{RESET}(p_i, v_{i,\text{ANC}}) \mid \forall i\}$  // Restore all particles to ancestor checkpoints
18:  else
19:    /* Uncertainty-aware redistribution */
20:     $p_{\text{WINNER}} \leftarrow \text{lex-argmax}_{p \in P, p.\text{ALIVE}}(p.R, U(p))$  // Best alive: max reward, break ties by uncertainty
21:    for each  $p_i \in P$  do
22:      if  $p_i$  is DEAD then
23:         $\text{RESET}(p_i, p_{\text{WINNER}})$  // Prune & respawn;  $p_i$  becomes alive after the reset
24:      end if
25:    end for
26:  end if
27: end for
28: /* Group consolidation (lexicographic ranking) */
29:  $p_{\text{WINNER}} \leftarrow \text{lex-argmax}_{p \in P}(p.R, U(p))$ 
30:  $P \leftarrow \{\text{RESET}(p_j, p_{\text{WINNER}}) \mid \forall j\}$  // Reset all particles to winner's checkpoint
31: return  $P, \mathcal{T}, U, p_{\text{WINNER}}$ 
```

all M groups based on the reward-uncertainty criterion in [Item 1 \(Algorithm 2, Line 16\)](#). The algorithm then compares each group’s maximum reward to the global winner’s. If a group’s best reward is strictly lower, all its particles are reset to the global winner ([Algorithm 2, Line 10](#)). If equal, the group continues its search independently. This mechanism balances diversity with efficiency: it allows competitive groups to explore unique trajectories while propagating breakthrough discoveries across the entire population.

4.4 Implementation Overview

We implement GOWU using a distributed coordinator-worker architecture that decouples environment simulation, population management, and uncertainty model training. Rollout workers stream observations into a shared replay buffer, from which a dedicated learner asynchronously trains the RND predictor ([Burda et al., 2018](#)) that instantiates the uncertainty oracle U . Particles select actions using a simple random policy: each particle commits to a single random action held fixed for the duration of each rollout segment. In the discrete setting, a different random action is played with small probability at each step ($\varepsilon = 0.2$). Full implementation details and model architectures are provided in [Appendix A](#).

Algorithm 2 GOWU: GO-WITH-UNCERTAINTY

input: Env. \mathcal{E} , iterations N_{iter} , number of groups M , and number of particles per group N

- 1: Initialize lineage tree \mathcal{T} with root node s_0 (initial state)
- 2: Initialize groups $\{G_1, \dots, G_M\}$, each with N particles, all starting at s_0
- 3: Initialize shared uncertainty estimator U
- 4: Initialize p_{winner} at state s_0 with cumulative reward 0
- 5: **for** $i = 1, \dots, N_{\text{iter}}$ **do**
- 6: **for each** Group G_m in parallel **do**
- 7: /* Global synchronization */
- 8: $p_m \leftarrow \text{lex-argmax}_{p \in G_m} (p.R, U(p))$
- 9: **if** $p_m.R < p_{\text{winner}}.R$ **then**
- 10: Reset G_m to the state of p_{winner} // Restore all particles to global winner’s checkpoint
- 11: **end if**
- 12: /* Evolve group */
- 13: $G_m, \mathcal{T}, U, p_m \leftarrow \text{EVOLVEGROUP}(G_m, \mathcal{T}, U)$ // Algorithm 1
- 14: **end for**
- 15: /* Update global winner */
- 16: $p_{\text{winner}} \leftarrow \text{lex-argmax}_{p \in \{p_1, \dots, p_M, p_{\text{winner}}\}} (p.R, U(p))$
- 17: **end for**

5 Experiments

We evaluate GOWU on two families of hard-exploration benchmarks spanning both discrete and continuous action spaces: Atari games (*Montezuma’s Revenge*, *Pitfall!*, and *Venture*) and MuJoCo continuous-control tasks (AntMaze and Adroit dexterous manipulation). Our experiments are designed to answer the following research questions:

- *RQ1 (Exploration efficiency)*: Can GOWU efficiently discover high-reward and task-completing trajectories across both discrete and continuous domains?
- *RQ2 (Quality of exploratory data)*: Can the discovered trajectories be distilled into deployable policies that achieve high scores (Atari) or high success rates (MuJoCo)?

Atari environments. We evaluate on *Montezuma’s Revenge*, *Pitfall!*, and *Venture*—three of the most challenging exploration benchmarks in the Arcade Learning Environment (ALE) (Bellemare et al., 2013; Machado et al., 2018). *Montezuma’s Revenge* requires long-horizon planning across multiple rooms, while *Pitfall!* presents a distinct challenge due to its very sparse rewards and visually similar rooms. Notably, *Pitfall!* remains largely unsolved without human demonstrations or domain knowledge (Ecoffet et al., 2021) when using sticky actions. *Venture* adds a distinct challenge: pursuing enemies imposing strict time pressure, requiring the agent to explore certain rooms *quickly*.

MuJoCo environments. To evaluate GOWU on continuous action spaces, we consider two families of tasks

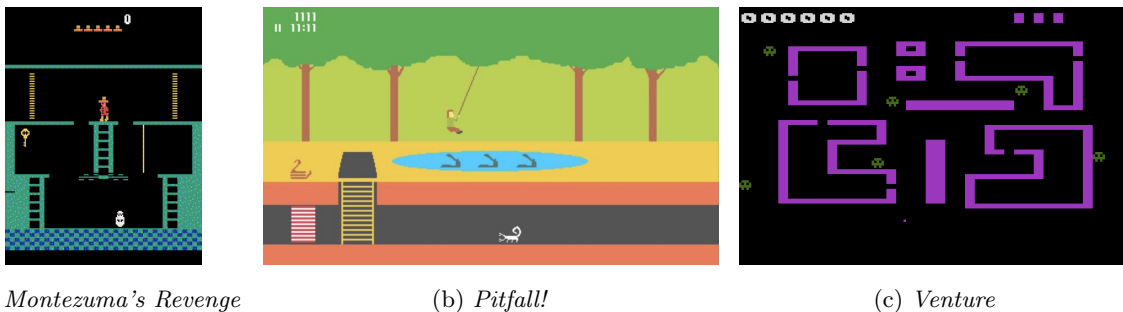


Figure 2: Fully rendered observations from the three hard-exploration Atari games used in our evaluation.

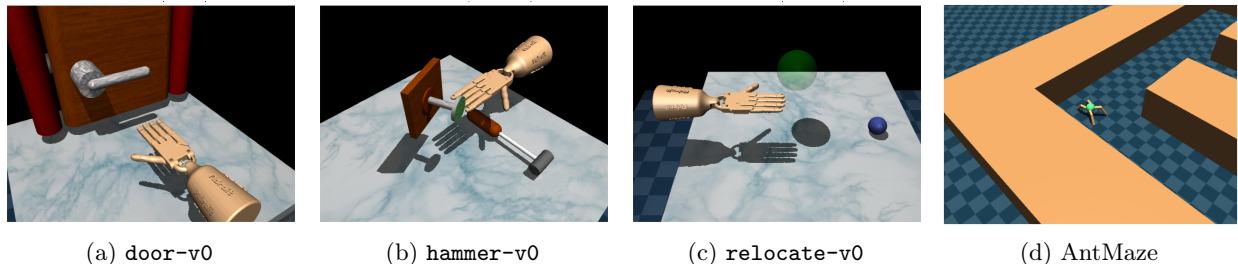


Figure 3: MuJoCo continuous-control tasks used in our evaluation. (a–c) Adroit dexterous manipulation tasks using the 24-DoF ShadowHand. (d) AntMaze navigation task (top-down view).

that require deep exploration from visual observations:

- *AntMaze* (*antmaze-large-diverse-v0*): A quadruped ant must navigate a large maze to reach a goal position. The environment provides only a sparse terminal reward upon reaching the goal (the default setting), requiring sustained exploration through extended corridors and dead ends.
- *Adroit* (*door-v0*, *hammer-v0*, *relocate-v0*): Dexterous manipulation tasks using the 24-degree-of-freedom ShadowHand (Rajeswaran et al., 2017). *door-v0* requires opening a door by its handle, *hammer-v0* requires picking up a hammer and driving a nail, and *relocate-v0* requires grasping a ball and moving it to a target location. The high dimensionality of the action space and the precision required for manipulation make these tasks extremely challenging. We enable the `sparse_reward` flag, which replaces the default dense reward shaping with a single task-completion reward.

Although the MuJoCo dynamics are deterministic, task configurations are randomized across seeds, preventing the policy from memorizing a fixed action sequence. For AntMaze, the target location is slightly randomized around the top-right corner of the maze. For *door-v0*, the position of the door and handle are perturbed across episodes; similarly, the nail position varies in *hammer-v0*. For *relocate-v0*, the randomization is more substantial: both the ball and target locations change significantly between seeds. We aim to solve all MuJoCo tasks *from images*: the final distilled policy receives only visual observations, not privileged state information.

Observations and environment configuration. Observations are processed into grayscale, frame-stacked images. For Atari, we follow the standard preprocessing pipeline (Mnih et al., 2015), producing $84 \times 84 \times 4$ observations. For MuJoCo, we render task-specific camera views at 120×120 and stack 4 consecutive frames; for AntMaze, an additional global top-down view of the maze is included (during Phase I, only this top-down view is used). All pixel values are normalized to $[0, 1]$. For the Atari environments, we use *sticky actions* ($p = 0.25$), introducing aleatoric stochasticity (Machado et al., 2018). For Atari and AntMaze, we use the standard action repeat of 4, where the selected action is applied 4 times; thus, each environment step consumes four game frames. Adroit tasks use no action repeat owing to the precision required for dexterous manipulation. Full details on observation processing are provided in Appendix E. Finally, we disable the *Pitfall!* timer during Phase I to enable non-episodic exploration; the timer is re-enabled during Phase II and evaluation (see Appendix D for details).

Exploration signals (Phase I). During Phase I, we define environment-specific DEAD state criteria—and, for MuJoCo, additional intermediate rewards—to guide particle redistribution in GOWU.

- *Atari*: We treat a loss of life—detected via a discount factor of zero—as a DEAD state. In *Pitfall!*, we additionally treat any negative reward (e.g., from touching a rolling barrel) as DEAD, since it signals an unrecoverable penalty. For *Montezuma’s Revenge*, we define an additional DEAD state to prevent exploitation of a newly discovered environment bug (see Appendix I).
- *AntMaze*: We define flipping over as a DEAD state, since the ant becomes irrecoverably stuck. See Appendix F for details on how this condition is extracted.
- *Adroit*: We define a single intermediate reward based on contact with the target surface: a reward of +1 is assigned when the hand first contacts the relevant object—the door handle, the hammer, or the ball. If contact is subsequently lost, we mark the particle as DEAD.

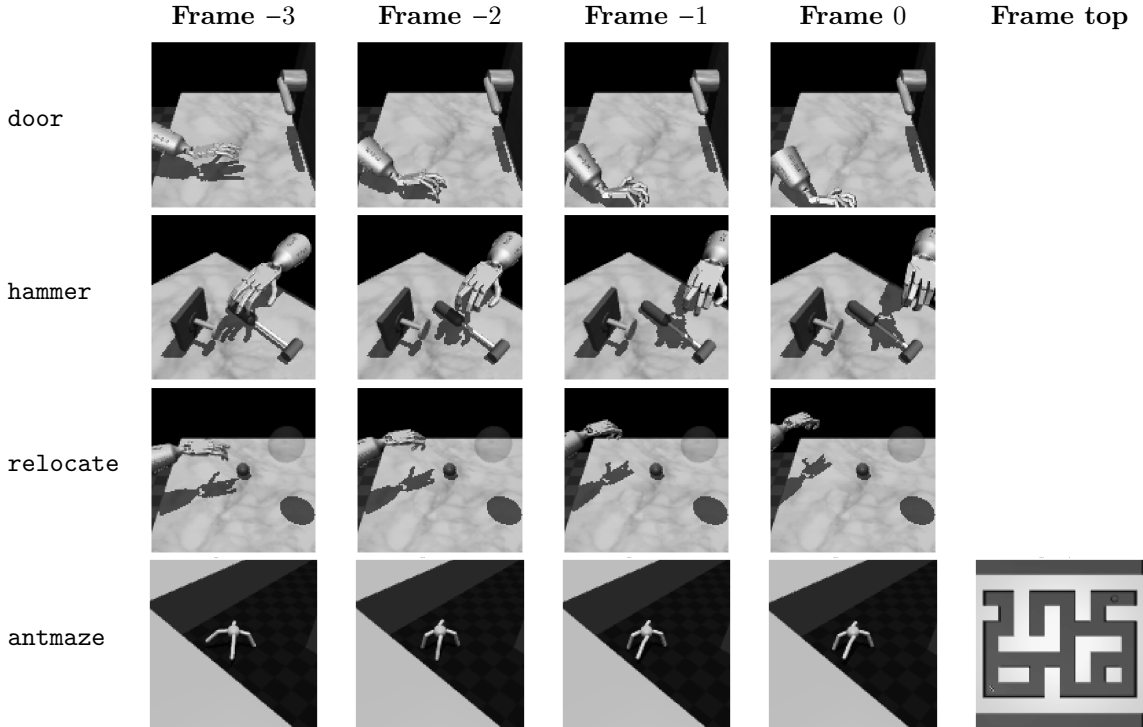


Figure 4: Processed visual observations as seen by the agent for each MuJoCo task. Each column shows a frame in the observation stack, from the oldest (Frame -3) to the most recent (Frame 0). For AntMaze, the “Frame top” column shows the global top-down view of the maze; during Phase I (exploration), only this top-down view is used. See [Section 5](#) for an overview and [Appendix E](#) for full details on the observation processing pipeline.

We emphasize that these signals are straightforwardly extracted from readily available state information and are far from the heavy reward shaping typically required by standard RL algorithms.

GowU parameters (Phase I). Population management parameters we use are listed in [Table 5](#).

Policy distillation (Phase II). Following the exploration phase, we distill the discovered trajectories into deployable policies using only the original environment rewards (the additional exploration signals from Phase I are not used). For each GowU run, we extract the highest-reward trajectory from the lineage tree ([Section 4.1](#)) and use it as a demonstration for a backward learning curriculum ([Salimans and Chen, 2018](#)). The agent is initialized near the end of the demonstration and trained using PPO ([Schulman et al., 2017](#)) to maximize cumulative reward from that point forward; as it masters the task, the initialization is progressively moved backward toward the start of the episode. For Atari, we decompose each demonstration into 10 segments delineated by reward events, training on all segments simultaneously; this decomposition breaks the long-horizon problem into manageable sub-tasks. For MuJoCo, no segmentation is applied and the goal location is held fixed to the one used during exploration while the curriculum progresses backward along a given demonstration. Once the curriculum reaches the initial state, the goal (i.e., the randomized target location and object placement described above) is allowed to vary across episodes, training the policy to generalize; using 10 demonstrations per Phase II run, each corresponding to a different goal configuration, provides initial diversity across goals. Throughout training, a background evaluator periodically fetches the latest policy weights and tracks the best-performing checkpoint. After training is complete, this checkpoint is evaluated on 500 rollouts to produce the final policy score.

See [Appendix B](#) for additional details on the curriculum strategy, environment-specific configurations, and evaluation procedures.

Baselines. For Atari, we compare against GO-EXPLORE (no domain knowledge) ([Ecoffet et al., 2021](#)), which

represents the current state of the art on hard-exploration games, and three intrinsic motivation methods: RND (Burda et al., 2018), MEME (Kapturowski et al., 2022) (AGENT57’s successor (Badia et al., 2020a)), and BYOL-HINDSIGHT (Jarrett et al., 2023). The latter two are among the strongest intrinsic motivation approaches for hard-exploration games.

For the MuJoCo tasks, direct baselines are unavailable. Existing methods for Adroit and AntMaze either rely on dense reward shaping, use privileged state observations, or operate in simpler settings. To the best of our knowledge, no prior method solves the adroit tasks from pixel observations in the sparse-reward setting without expert demonstrations. We discuss this further in Appendix H.

5.1 Phase I Results: Exploration Efficiency of GowU

Table 1: Comparison of GowU against baselines on hard-exploration Atari games. For GowU, we report the mean (\pm standard deviation) cumulative reward along the discovered demonstrations across 100 exploration seeds after at most 600M frames per seed, and the mean (\pm standard deviation) policy score across 10 Phase II runs (see Table 3 for full statistics). All results use sticky actions ($p = 0.25$), except GO-EXPLORE, which uses a deterministic environment during exploration. Baseline numbers are taken from the respective papers. *BYOL-HINDSIGHT values are approximate, extracted visually from Figure 19 in the original paper.

GAME	OURS		GO-EXPLORE	RND	MEME	BYOL-HIND.
	EXPLORATION (GowU)	ROBUSTIFICATION				
MONTEZUMA	98,249 \pm 18,102	196,312 \pm 49,670	43,791	8,152	9,429	\sim 14,517*
PITFALL	54,440 \pm 14,817	101,972 \pm 2,226	6,945	-3	7,821	\sim 16,211*
VENTURE	5,012 \pm 2,678	6,436 \pm 1,504	2,281	1,859	2,583	\sim 2,328*

We run GowU for 100 seeds on each Atari game—400M frames per seed for *Montezuma’s Revenge* and 600M for *Pitfall!* and *Venture*—to evaluate exploration efficiency. Table 1 summarizes the mean cumulative reward at the end of exploration alongside the baselines, and Figure 5 compares the GowU and GO-EXPLORE (Ecoffet et al., 2021) exploration curves on each game. Across all three games, GowU discovers high-scoring trajectories substantially faster: it reaches higher cumulative rewards within a fraction of the frames required by GO-EXPLORE.

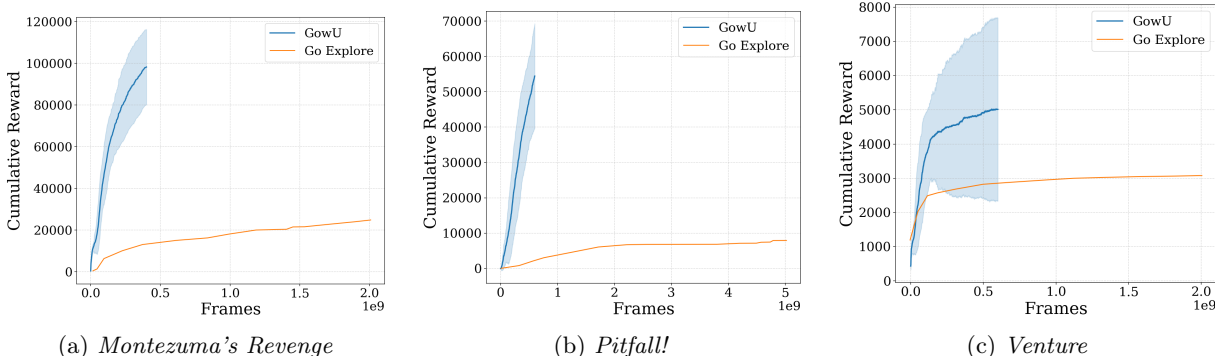


Figure 5: Phase I exploration on Atari: GowU vs. GO-EXPLORE (Ecoffet et al., 2021). Mean cumulative reward (\pm std) across 100 seeds as a function of game frames. GO-EXPLORE curves are approximated from Extended Data Fig. 2 in (Ecoffet et al., 2021).

We next evaluate whether this efficiency extends to continuous control. Table 2 reports statistics on the number of environment frames required for GowU to discover a task-completing trajectory across 100 Phase I seeds for each MuJoCo task. All tasks are solved reliably and efficiently (using substantially fewer frames than in the Atari setting).

Table 2: MuJoCo Phase I exploration efficiency: number of environment frames until a task-completing trajectory is first discovered, across 100 GowU seeds.

TASK	MEAN	STD	MEDIAN	MIN	MAX
HAMMER	26,797	13,983	24,142	4,713	73,306
DOOR	272,688	200,824	224,338	17,086	943,066
RELOCATE	275,372	839,815	69,546	2,137	8,015,087
ANTMAZE	10,161,272	6,697,736	8,517,186	3,078,412	48,332,904

5.2 Phase II Results: Policy Distillation

Following the exploration phase, we distill the discovered trajectories into deployable policies via the backward learning curriculum described in Section 5. For each task, we conduct 10 Phase II runs, where each run trains on a unique set of 10 demonstrations, each extracted from a different GowU exploration run. Each Phase II run is repeated with 5 random seeds, and its result is averaged over the seeds. We note that unlike the demonstrations used for backward learning in (Salimans and Chen, 2018; Ecoffet et al., 2021), which consist of a checkpoint at every environment step, ours consist of checkpoints spaced INNER STEPS apart, since we only expand the tree at the end of each rollout (see Algorithm 1). Despite the gaps between checkpoints, the backward algorithm successfully learns high-performing policies.

Table 3: Detailed Phase II robustification statistics for GowU on Atari. We conduct 10 Phase II runs per game, where each run trains on a unique set of 10 demonstrations, each from a different exploration run. Each Phase II run is repeated with 5 random seeds, and its result is averaged over the seeds. We report the mean, standard deviation, median, worst-run, and best-run policy scores across the 10 runs.

GAME	MEAN	STD	MEDIAN	WORST-RUN	BEST-RUN
MONTEZUMA	196,312	49,670	189,151	130,501	263,111
PITFALL	101,972	2,226	102,296	97,090	105,589
VENTURE	6,436	1,504	6,177	4,743	9,357

For Atari, the robustification column of Table 1 reports the mean policy scores (\pm standard deviation) across the 10 Phase II runs; full statistics are provided in Table 3. GowU’s distilled policies surpass all baselines on every game by a wide margin. For *Montezuma’s Revenge*, the best run achieves 263,111. Across all games, even the worst-run scores remain substantially above the baselines.

For the MuJoCo tasks, we evaluate the distilled policies by their success rate: 100.0% \pm 0.1 on **hammer**, 98.1% \pm 0.6 on **door**, 95.2% \pm 1.7 on **relocate**, and 96.1% \pm 1.9 on **AntMaze** (see Table 4 for full statistics). To the best of our knowledge, no prior method has achieved comparable success rates on these tasks from pixel observations with sparse rewards, without expert demonstrations (see Appendix H for a detailed discussion of existing approaches).

Table 4: Phase II success rate statistics for MuJoCo tasks. We conduct 10 Phase II runs per task, where each run trains on a unique set of 10 demonstrations and is repeated with 5 random seeds, and its result is averaged over the seeds. We report the mean, standard deviation, median, worst-run, and best-run success rates across the 10 runs.

TASK	MEAN	STD	MEDIAN	WORST-RUN	BEST-RUN
HAMMER	1.000	0.001	1.000	0.997	1.000
DOOR	0.981	0.006	0.981	0.972	0.992
RELOCATE	0.952	0.017	0.947	0.933	0.973
ANTMAZE	0.961	0.019	0.964	0.916	0.980

We report the Phase II frame budgets in Section B.6; in all cases, the cost of policy distillation far exceeds

that of Phase I, making exploration, with our approach, effectively the easier part.

5.3 Ablation Study

We conduct ablation experiments on *Montezuma’s Revenge* to validate the key design choices of GOWU (see [Appendix G](#) for details). Four findings stand out: (1) removing the uncertainty-based winner selection causes exploration to fail, confirming that uncertainty is essential for directing the search; (2) disabling group consolidation also degrades performance, though the variant still performs better than the no-uncertainty ablation; (3) we vary the number of parallel groups $M \in \{1, 2, 4, 8\}$ while keeping the total particle count fixed—2 and 4 groups yield similar performance, while a single group is the worst and 8 groups degrades due to too few particles per group; and (4) GOWU randomizes its search hyperparameters at each step by default; comparing this against fixing them for the entire run confirms that per-iteration randomization provides robust performance without requiring careful tuning.

5.4 Discussion and Future Work

Our findings suggest that GWTW-style particle-based tree search guided by a measure of uncertainty is a highly promising paradigm for solving hard-exploration tasks. Although particle-based methods that search directly in state space have received limited attention in the context of deep exploration in Atari and robotics simulation, they have gained significant traction in the LLM setting. A growing body of work uses populations of partial generations—steered via resampling—to guide language model outputs toward desired properties ([Lew et al., 2023](#); [Zhao et al., 2024](#); [Feng et al., 2024](#); [Lipkin et al., 2025](#); [Loula et al., 2025](#); [Grand et al., 2025](#); [Puri et al., 2025](#)). [Golowich et al. \(2026\)](#) frame these methods as Sequential Monte Carlo and provide theoretical guarantees. In these approaches, a process reward model typically drives the resampling step; an interesting direction would be to replace it with an uncertainty-based signal, as in GOWU. More broadly, the LLM setting is especially well-suited to our framework’s reset primitive, since the “environment” is a token sequence and resetting merely entails restoring a context window ([Foster et al., 2025](#); [Chang et al., 2024](#)).

In another direction, by bypassing the need for shaped rewards or expert demonstrations, GOWU could open the door to scaling up open-ended robotic learning in simulation ([Team et al., 2021](#)), where resets are readily available and leveraging them effectively is crucial ([Mhammedi et al., 2024](#)).

On the methodological side, an important direction is the design of more principled uncertainty measures. RND is scalable and effective in our setting ([Burda et al., 2018](#)), but can still assign persistently high novelty to stochastic observations ([Mavor-Parker et al., 2022](#)). Promising alternatives include learned representations that explicitly disentangle aleatoric and epistemic uncertainty ([Jarrett et al., 2023](#)), as well as temporal contrastive features that capture temporal structure and may provide a stronger basis for noise-robust exploration (see [Appendix H](#)).

Acknowledgments

We thank Arkanath Pathak for discussions during the early stages of this project.

References

- Ilge Akkaya, Marcin Andrychowicz, Maciek Chociej, Mateusz Litwin, Bob McGrew, Arthur Petron, Alex Paino, Matthias Plappert, Glenn Powell, Raphael Ribas, et al. Solving rubik’s cube with a robot hand. *arXiv preprint arXiv:1910.07113*, 2019.
- David Aldous and Umesh Vazirani. “go with the winners” algorithms. In *Proceedings 35th Annual Symposium on Foundations of Computer Science*, pages 492–501. IEEE, 1994.
- Elie Aljalbout, Jiaxu Xing, Angel Romero, Iretoiyo Akinola, Caelan Reed Garrett, Eric Heiden, Abhishek Gupta, Tucker Hermans, Yashraj Narang, Dieter Fox, et al. The reality gap in robotics: Challenges, solutions, and best practices. *Annual Review of Control, Robotics, and Autonomous Systems*, 9, 2025.
- Adrià Puigdomènech Badia, Bilal Piot, Steven Kapturowski, Pablo Sprechmann, Alex Vitvitskyi, Zhao-han Daniel Guo, and Charles Blundell. Agent57: Outperforming the atari human benchmark. In *International conference on machine learning*, pages 507–517. PMLR, 2020a.
- Adrià Puigdomènech Badia, Pablo Sprechmann, Alex Vitvitskyi, Daniel Guo, Bilal Piot, Steven Kapturowski, Olivier Tieleman, Martín Arjovsky, Alexander Pritzel, Andrew Bolt, et al. Never give up: Learning directed exploration strategies. *arXiv preprint arXiv:2002.06038*, 2020b.
- Mayank Bansal, Alex Krizhevsky, and Abhijit Ogale. Chauffeurnet: Learning to drive by imitating the best and synthesizing the worst. *arXiv preprint arXiv:1812.03079*, 2018.
- Andrew G Barto. Intrinsic motivation and reinforcement learning. In *Intrinsically motivated learning in natural and artificial systems*, pages 17–47. Springer, 2012.
- Marc Bellemare, Sriram Srinivasan, Georg Ostrovski, Tom Schaul, David Saxton, and Remi Munos. Unifying count-based exploration and intrinsic motivation. *Advances in neural information processing systems*, 29, 2016.
- Marc G Bellemare, Yavar Naddaf, Joel Veness, and Michael Bowling. The arcade learning environment: An evaluation platform for general agents. *Journal of artificial intelligence research*, 47:253–279, 2013.
- Mariusz Bojarski, Davide Del Testa, Daniel Dworakowski, Bernhard Firner, Beat Flepp, Prasoon Goyal, Lawrence D Jackel, Mathew Monfort, Urs Muller, Jiakai Zhang, et al. End to end learning for self-driving cars. *arXiv preprint arXiv:1604.07316*, 2016.
- Michał Bortkiewicz, Władysław Pałucki, Vivek Myers, Tadeusz Dziarmaga, Tomasz Arczewski, Łukasz Kuciński, and Benjamin Eysenbach. Accelerating goal-conditioned rl algorithms and research. *arXiv preprint arXiv:2408.11052*, 2024.
- Anthony Brohan, Noah Brown, Justice Carbajal, Yevgen Chebotar, Joseph Dabis, Chelsea Finn, Keerthana Gopalakrishnan, Karol Hausman, Alex Herzog, Jasmine Hsu, et al. Rt-1: Robotics transformer for real-world control at scale. *arXiv preprint arXiv:2212.06817*, 2022.
- Yuri Burda, Harrison Edwards, Amos Storkey, and Oleg Klimov. Exploration by random network distillation. *arXiv preprint arXiv:1810.12894*, 2018.
- Jonathan D Chang, Wenhao Zhan, Owen Oertell, Kianté Brantley, Dipendra Misra, Jason D Lee, and Wen Sun. Dataset reset policy optimization for rlhf. *arXiv preprint arXiv:2404.08495*, 2024.
- Paul F Christiano, Jan Leike, Tom Brown, Miljan Martic, Shane Legg, and Dario Amodei. Deep reinforcement learning from human preferences. *Advances in neural information processing systems*, 30, 2017.

- Edoardo Conti, Vashisht Madhavan, Felipe Petroski Such, Joel Lehman, Kenneth O. Stanley, and Jeff Clune. Improving exploration in evolution strategies for deep reinforcement learning via a population of novelty-seeking agents. In *Advances in Neural Information Processing Systems*, 2018.
- Adrien Couëtoux, Jean-Baptiste Hoock, Nataliya Sokolovska, Olivier Teytaud, and Nicolas Bonnard. Continuous upper confidence trees. In *International conference on learning and intelligent optimization*, pages 433–445. Springer, 2011.
- Rémi Coulom. Efficient selectivity and backup operators in monte-carlo tree search. In *International conference on computers and games*, pages 72–83. Springer, 2006.
- Stefan Depeweg, Jose-Miguel Hernandez-Lobato, Finale Doshi-Velez, and Steffen Udluft. Decomposition of uncertainty in bayesian deep learning for efficient and risk-sensitive learning. In *International conference on machine learning*, pages 1184–1193. PMLR, 2018.
- Adrien Ecoffet, Joost Huizinga, Joel Lehman, Kenneth O Stanley, and Jeff Clune. Go-explore: a new approach for hard-exploration problems. *arXiv preprint arXiv:1901.10995*, 2019.
- Adrien Ecoffet, Joost Huizinga, Joel Lehman, Kenneth O Stanley, and Jeff Clune. First return, then explore. *Nature*, 590(7847):580–586, 2021.
- Lasse Espeholt, Hubert Soyer, Remi Munos, Karen Simonyan, Vlad Mnih, Tom Ward, Yotam Doron, Vlad Firoiu, Tim Harley, Iain Dunning, et al. Impala: Scalable distributed deep-rl with importance weighted actor-learner architectures. In *International conference on machine learning*, pages 1407–1416. PMLR, 2018.
- Benjamin Eysenbach, Shixiang Gu, Julian Ibarz, and Sergey Levine. Leave no trace: Learning to reset for safe and autonomous reinforcement learning. *arXiv preprint arXiv:1711.06782*, 2017.
- Benjamin Eysenbach, Abhishek Gupta, Julian Ibarz, and Sergey Levine. Diversity is all you need: Learning skills without a reward function. *arXiv preprint arXiv:1802.06070*, 2018.
- Shengyu Feng, Xiang Kong, Shuang Ma, Aonan Zhang, Dong Yin, Chong Wang, Ruoming Pang, and Yiming Yang. Step-by-step reasoning for math problems via twisted sequential monte carlo. *arXiv preprint arXiv:2410.01920*, 2024.
- Dylan J Foster, Zakaria Mhammedi, and Dhruv Rohatgi. Is a good foundation necessary for efficient reinforcement learning? the computational role of the base model in exploration. In *The Thirty Eighth Annual Conference on Learning Theory*, pages 2026–2142. PMLR, 2025.
- Justin Fu, Aviral Kumar, Ofir Nachum, George Tucker, and Sergey Levine. D4rl: Datasets for deep data-driven reinforcement learning. *arXiv preprint arXiv:2004.07219*, 2020.
- Quentin Gallouédec and Emmanuel Dellandréa. Cell-free latent go-explore. In *International Conference on Machine Learning*, pages 10571–10586. PMLR, 2023.
- Noah Golowich, Fan Chen, Dhruv Rohatgi, Raghav Singhal, Carles Domingo-Enrich, Dylan J Foster, and Akshay Krishnamurthy. Reject, resample, repeat: Understanding parallel reasoning in language model inference. *arXiv preprint arXiv:2603.07887*, 2026.
- Gabriel Grand, Joshua B Tenenbaum, Vikash K Mansinghka, Alexander K Lew, and Jacob Andreas. Self-steering language models. *arXiv preprint arXiv:2504.07081*, 2025.
- Zhaohan Guo, Shantanu Thakoor, Miruna Pislar, Bernardo Avila Pires, Florent Alché, Corentin Tallec, Alaa Saade, Daniele Calandriello, Jean-Bastien Grill, Yunhao Tang, et al. Byol-explore: Exploration by bootstrapped prediction. *Advances in neural information processing systems*, 35:31855–31870, 2022.
- Abhishek Gupta, Justin Yu, Tony Z Zhao, Vikash Kumar, Aaron Rovinsky, Kelvin Xu, Thomas Devlin, and Sergey Levine. Reset-free reinforcement learning via multi-task learning: Learning dexterous manipulation behaviors without human intervention. In *2021 IEEE international conference on robotics and automation (ICRA)*, pages 6664–6671. IEEE, 2021.

- Danijar Hafner, Kuang-Huei Lee, Ian Fischer, and Pieter Abbeel. Deep hierarchical planning from pixels. *Advances in Neural Information Processing Systems*, 35:26091–26104, 2022.
- Todd Hester, Matej Vecerik, Olivier Pietquin, Marc Lanctot, Tom Schaul, Bilal Piot, Dan Horgan, John Quan, Andrew Sendonaris, Ian Osband, et al. Deep q-learning from demonstrations. In *Proceedings of the AAAI conference on artificial intelligence*, volume 32, 2018.
- Rein Houthoofd, Xi Chen, Yan Duan, John Schulman, Filip De Turck, and Pieter Abbeel. Vime: Variational information maximizing exploration. In *Advances in Neural Information Processing Systems*, volume 29, 2016.
- Suning Huang, Zheyu Aqa Zhang, Tianhai Liang, Yihan Xu, Zhehao Kou, Chenhao Lu, Guowei Xu, Zhengrong Xue, and Huazhe Xu. Mentor: Mixture-of-experts network with task-oriented perturbation for visual reinforcement learning. In *International Conference on Machine Learning*, pages 26143–26161. PMLR, 2025.
- Daniel Jarrett, Corentin Tallec, Florent Altché, Thomas Mesnard, Remi Munos, and Michal Valko. Curiosity in hindsight: Intrinsic exploration in stochastic environments. In *International Conference on Machine Learning*, pages 14780–14816. PMLR, 2023.
- Chi Jin, Akshay Krishnamurthy, Max Simchowitz, and Tiancheng Yu. Reward-free exploration for reinforcement learning. In *International Conference on Machine Learning*, pages 4870–4879. PMLR, 2020.
- Steven Kapturowski, Víctor Campos, Ray Jiang, Nemanja Rakićević, Hado van Hasselt, Charles Blundell, and Adria Puigdomenech Badia. Human-level atari 200x faster. *arXiv preprint arXiv:2209.07550*, 2022.
- Michael Kearns and Satinder Singh. Near-optimal reinforcement learning in polynomial time. *Machine learning*, 49(2):209–232, 2002.
- Alex Kendall and Yarin Gal. What uncertainties do we need in bayesian deep learning for computer vision? *Advances in neural information processing systems*, 30, 2017.
- Junsu Kim, Younggyo Seo, and Jinwoo Shin. Landmark-guided subgoal generation in hierarchical reinforcement learning. *Advances in neural information processing systems*, 34:28336–28349, 2021.
- Levente Kocsis and Csaba Szepesvári. Bandit based monte-carlo planning. In *European conference on machine learning*, pages 282–293. Springer, 2006.
- Balaji Lakshminarayanan, Alexander Pritzel, and Charles Blundell. Simple and scalable predictive uncertainty estimation using deep ensembles. *Advances in neural information processing systems*, 30, 2017.
- Michael Laskin, Denis Yarats, Hao Liu, Kimin Lee, Albert Zhan, Kevin Lu, Catherine Cang, Lerrel Pinto, and Pieter Abbeel. Urlb: Unsupervised reinforcement learning benchmark. *arXiv preprint arXiv:2110.15191*, 2021.
- Joel Lehman and Kenneth O Stanley. Abandoning objectives: Evolution through the search for novelty alone. *Evolutionary computation*, 19(2):189–223, 2011.
- Alexander K Lew, Tan Zhi-Xuan, Gabriel Grand, and Vikash K Mansinghka. Sequential monte carlo steering of large language models using probabilistic programs. *arXiv preprint arXiv:2306.03081*, 2023.
- Gen Li, Yuxin Chen, Yuejie Chi, Yuantao Gu, and Yuting Wei. Sample-efficient reinforcement learning is feasible for linearly realizable mdps with limited revisiting. *Advances in Neural Information Processing Systems*, 34:16671–16685, 2021.
- Benjamin Lipkin, Benjamin LeBrun, Jacob Hoover Vigly, João Loula, David R MacIver, Li Du, Jason Eisner, Ryan Cotterell, Vikash Mansinghka, Timothy J O’Donnell, et al. Fast controlled generation from language models with adaptive weighted rejection sampling. *arXiv preprint arXiv:2504.05410*, 2025.

- Grace Liu, Michael Tang, and Benjamin Eysenbach. A single goal is all you need: Skills and exploration emerge from contrastive rl without rewards, demonstrations, or subgoals. *arXiv preprint arXiv:2408.05804*, 2024.
- Hao Liu and Pieter Abbeel. Behavior from the void: Unsupervised active pre-training. *Advances in Neural Information Processing Systems*, 34:18459–18473, 2021.
- João Loula, Benjamin LeBrun, Li Du, Ben Lipkin, Clemente Pasti, Gabriel Grand, Tianyu Liu, Yahya Emara, Marjorie Freedman, Jason Eisner, et al. Syntactic and semantic control of large language models via sequential monte carlo. *arXiv preprint arXiv:2504.13139*, 2025.
- Marlos C Machado, Marc G Bellemare, Erik Talvitie, Joel Veness, Matthew Hausknecht, and Michael Bowling. Revisiting the arcade learning environment: Evaluation protocols and open problems for general agents. *Journal of Artificial Intelligence Research*, 61:523–562, 2018.
- Augustine Mavor-Parker, Kimberly Young, Caswell Barry, and Lewis Griffin. How to stay curious while avoiding noisy tvs using aleatoric uncertainty estimation. In *International conference on machine learning*, pages 15220–15240. PMLR, 2022.
- Zak Mhammedi, Adam Block, Dylan J Foster, and Alexander Rakhlin. Efficient model-free exploration in low-rank mdps. *Advances in Neural Information Processing Systems*, 36:66782–66817, 2023a.
- Zakaria Mhammedi, Dylan J Foster, and Alexander Rakhlin. Representation learning with multi-step inverse kinematics: An efficient and optimal approach to rich-observation rl. In *International Conference on Machine Learning*, pages 24659–24700. PMLR, 2023b.
- Zakaria Mhammedi, Dylan J Foster, and Alexander Rakhlin. The power of resets in online reinforcement learning. *Advances in Neural Information Processing Systems*, 37:12334–12407, 2024.
- Dipendra Misra, Mikael Henaff, Akshay Krishnamurthy, and John Langford. Kinematic state abstraction and provably efficient rich-observation reinforcement learning. In *International conference on machine learning*, pages 6961–6971. PMLR, 2020.
- Volodymyr Mnih, Koray Kavukcuoglu, David Silver, Andrei A Rusu, Joel Veness, Marc G Bellemare, Alex Graves, Martin Riedmiller, Andreas K Fidjeland, Georg Ostrovski, et al. Human-level control through deep reinforcement learning. *nature*, 518(7540):529–533, 2015.
- Faisal Mohamed, Catherine Ji, Benjamin Eysenbach, and Glen Berseth. Temporal representations for exploration: Learning complex exploratory behavior without extrinsic rewards. *arXiv preprint arXiv:2603.02008*, 2026.
- Shakir Mohamed and Danilo Jimenez Rezende. Variational information maximisation for intrinsically motivated reinforcement learning. *Advances in neural information processing systems*, 28, 2015.
- Jean-Baptiste Mouret and Jeff Clune. Illuminating search spaces by mapping elites. *arXiv preprint arXiv:1504.04909*, 2015.
- Vivek Myers, Chongyi Zheng, Anca Dragan, Sergey Levine, and Benjamin Eysenbach. Learning temporal distances: Contrastive successor features can provide a metric structure for decision-making. In *International Conference on Machine Learning*, pages 37076–37096. PMLR, 2024.
- Yaniv Oren, Villiam Vadocz, Matthijs TJ Spaan, and Wendelin Böhmer. Epistemic monte carlo tree search. *arXiv preprint arXiv:2210.13455*, 2022.
- Ian Osband, Charles Blundell, Alexander Pritzel, and Benjamin Van Roy. Deep exploration via bootstrapped dqn. In *Advances in Neural Information Processing Systems*, volume 29, 2016.
- Ian Osband, John Aslanides, and Albin Cassirer. Randomized prior functions for deep reinforcement learning. *Advances in neural information processing systems*, 31, 2018.

- Pierre-Yves Oudeyer, Frdric Kaplan, and Verena V Hafner. Intrinsic motivation systems for autonomous mental development. *IEEE transactions on evolutionary computation*, 11(2):265–286, 2007.
- Long Ouyang, Jeffrey Wu, Xu Jiang, Diogo Almeida, Carroll Wainwright, Pamela Mishkin, Chong Zhang, Sandhini Agarwal, Katarina Slama, Alex Ray, et al. Training language models to follow instructions with human feedback. *Advances in neural information processing systems*, 35:27730–27744, 2022.
- Jack Parker-Holder, Aldo Pacchiano, Krzysztof M Choromanski, and Stephen J Roberts. Effective diversity in population based reinforcement learning. *Advances in Neural Information Processing Systems*, 33: 18050–18062, 2020.
- Deepak Pathak, Pulkit Agrawal, Alexei A Efros, and Trevor Darrell. Curiosity-driven exploration by self-supervised prediction. In *International conference on machine learning*, pages 2778–2787. PMLR, 2017.
- Deepak Pathak, Dhiraj Gandhi, and Abhinav Gupta. Self-supervised exploration via disagreement. In *International conference on machine learning*, pages 5062–5071. PMLR, 2019.
- Justin K Pugh, Lisa B Soros, and Kenneth O Stanley. Quality diversity: A new frontier for evolutionary computation. *Frontiers in Robotics and AI*, 3:40, 2016.
- Isha Puri, Shivchander Sudalairaj, Guangxuan Xu, Kai Xu, and Akash Srivastava. A probabilistic inference approach to inference-time scaling of llms using particle-based monte carlo methods. *arXiv e-prints*, pages arXiv–2502, 2025.
- Mohammed Abu Qassem, Iyad Abuhadrous, and Hatem Elaydi. Modeling and simulation of 5 dof educational robot arm. In *2010 2nd International Conference on Advanced Computer Control*, volume 5, pages 569–574. IEEE, 2010.
- Rafael Rafailov, Archit Sharma, Eric Mitchell, Christopher D Manning, Stefano Ermon, and Chelsea Finn. Direct preference optimization: Your language model is secretly a reward model. *Advances in neural information processing systems*, 36:53728–53741, 2023.
- Aravind Rajeswaran, Vikash Kumar, Abhishek Gupta, Giulia Vezzani, John Schulman, Emanuel Todorov, and Sergey Levine. Learning complex dexterous manipulation with deep reinforcement learning and demonstrations. *arXiv preprint arXiv:1709.10087*, 2017.
- Tim Salimans and Richard Chen. Learning montezuma’s revenge from a single demonstration. *arXiv preprint arXiv:1812.03381*, 2018.
- Jürgen Schmidhuber. Curious model-building control systems. In *Proc. international joint conference on neural networks*, pages 1458–1463, 1991.
- John Schulman, Filip Wolski, Prafulla Dhariwal, Alec Radford, and Oleg Klimov. Proximal policy optimization algorithms, 2017. arXiv preprint arXiv:1707.06347.
- Ramanan Sekar, Oleh Rybkin, Kostas Daniilidis, Pieter Abbeel, Danijar Hafner, and Deepak Pathak. Planning to explore via self-supervised world models. In *International conference on machine learning*, pages 8583–8592. PMLR, 2020.
- Pranav Shyam, Wojciech Jaśkowski, and Faustino Gomez. Model-based active exploration. In *International conference on machine learning*, pages 5779–5788. PMLR, 2019.
- David Silver, Aja Huang, Chris J Maddison, Arthur Guez, Laurent Sifre, George Van Den Driessche, Julian Schrittwieser, Ioannis Antonoglou, Veda Panneershelvam, Marc Lanctot, et al. Mastering the game of go with deep neural networks and tree search. *nature*, 529(7587):484–489, 2016.
- David Silver, Thomas Hubert, Julian Schrittwieser, Ioannis Antonoglou, Matthew Lai, Arthur Guez, Marc Lanctot, Laurent Sifre, Dhharshan Kumaran, Thore Graepel, et al. A general reinforcement learning algorithm that masters chess, shogi, and go through self-play. *Science*, 362(6419):1140–1144, 2018.

- Bradly C Stadie, Sergey Levine, and Pieter Abbeel. Incentivizing exploration in reinforcement learning with deep predictive models. *arXiv preprint arXiv:1507.00814*, 2015.
- Open Ended Learning Team, Adam Stooke, Anuj Mahajan, Catarina Barros, Charlie Deck, Jakob Bauer, Jakub Sygnowski, Maja Trebacz, Max Jaderberg, Michael Mathieu, et al. Open-ended learning leads to generally capable agents. *arXiv preprint arXiv:2107.12808*, 2021.
- Josh Tobin, Rachel Fong, Alex Ray, Jonas Schneider, Wojciech Zaremba, and Pieter Abbeel. Domain randomization for transferring deep neural networks from simulation to the real world. In *2017 IEEE/RSJ international conference on intelligent robots and systems (IROS)*, pages 23–30. IEEE, 2017.
- Jianren Wang, Yifan Su, Abhinav Gupta, and Deepak Pathak. Evolutionary policy optimization. *arXiv preprint arXiv:2503.19037*, 2025.
- Yibo Wang and Jiang Zhao. Learning off-policy with model-based intrinsic motivation for active online exploration. *arXiv preprint arXiv:2404.00651*, 2024.
- Guowei Xu, Ruijie Zheng, Yongyuan Liang, Xiyao Wang, Zhecheng Yuan, Tianying Ji, Yu Luo, Xiaoyu Liu, Jiaxin Yuan, Pu Hua, et al. Drm: Mastering visual reinforcement learning through dormant ratio minimization. *arXiv preprint arXiv:2310.19668*, 2023.
- Dong Yin, Sridhar Thiagarajan, Nevena Lazic, Nived Rajaraman, Botao Hao, and Csaba Szepesvari. Sample efficient deep reinforcement learning via local planning. *arXiv preprint arXiv:2301.12579*, 2023.
- Stephen Zhao, Rob Brekelmans, Alireza Makhzani, and Roger Grosse. Probabilistic inference in language models via twisted sequential monte carlo. *arXiv preprint arXiv:2404.17546*, 2024.
- Wenshuai Zhao, Jorge Peña Queraltá, and Tomi Westerlund. Sim-to-real transfer in deep reinforcement learning for robotics: a survey. In *2020 IEEE symposium series on computational intelligence (SSCI)*, pages 737–744. IEEE, 2020.

Appendix Table of Contents

A Implementation Details for GowU	21
A.1 Central Coordinator	21
A.2 Distributed Rollout Workers	21
A.3 RND Learner	21
A.4 Population Management Hyperparameters	22
A.5 Computational Resources	22
B Implementation Details for the Backward Algorithm	22
B.1 Overview and segmentation	23
B.2 Curriculum strategy	23
B.3 Environment-specific configurations	24
B.4 Agent architecture	24
B.5 Hyperparameters and configuration	24
B.6 Evaluation	25
C Environment Checkpointing	26
D Pitfall Timer	26
E Observation Processing	26
E.1 Atari	26
E.2 Adroit	27
E.3 AntMaze	28
F MuJoCo Reward and Dead-State Extraction	28
F.1 AntMaze: Flip Detection	28
F.2 Adroit: Sparse Contact Rewards	28
G Ablation Study	29
H Additional Related Works	30
I <i>Montezuma’s Revenge</i> Middle Room Bug	31
J <i>Montezuma’s Revenge</i> Key Respawn Mechanism	32
K Why GWTW is Exponentially Faster: A Concrete Example	32

A Implementation Details for GowU

This appendix provides full implementation details for the distributed architecture summarized in [Section 4.4](#), including the uncertainty estimator architecture and training procedure. The system decouples environment simulation, population management, and uncertainty model training, enabling high-throughput exploration. It consists of three logical components communicating asynchronously: a *central coordinator*, a pool of *distributed rollout workers*, and a dedicated *RND learner*.

A.1 Central Coordinator

The central coordinator acts as the orchestrator of the search. It manages the global state of the population and coordinates the branches of exploration. Its responsibilities are as follows:

Population state management. The coordinator tracks the status of all $M \times N$ particles, including each particle’s current environment checkpoint, cumulative reward, and survival status (ALIVE or DEAD, as defined in [Section 3](#)).

State-lineage tree maintenance. The coordinator hosts the global state-lineage tree ([Section 4.1](#)) and is responsible for expanding it with new nodes as workers report completed rollouts. Each node stores the environment checkpoint, cumulative reward, and a parent pointer. To extract a demonstration path for Phase II, we select the highest-reward leaf and traverse the parent pointers upward, collecting the environment checkpoint and cumulative reward at each node.

The Go-With-The-Winner loop. The coordinator drives the top-level iterations of the GWTW loop ([Algorithm 2](#)). Each iteration proceeds in three phases:

1. **Dispatch:** The coordinator issues remote procedure calls (RPCs) to trigger rollouts on the worker pool, providing each worker with the starting checkpoint and group index.
2. **Aggregate:** It waits for all parallel rollouts to complete and collects the resulting endpoints, trajectories, and rewards.
3. **Sync and prune:** The coordinator applies the winner-selection and pruning logic ([Section 4.2](#)) and instructs the workers to overwrite failing particles with clones of the winners.

A.2 Distributed Rollout Workers

The workers are parallel execution nodes that drive environment interactions. They act as stateless clients that execute directives issued by the coordinator.

State restoration. Each worker receives a compact environment snapshot (checkpoint) from the global lineage tree and restores the local simulator to that exact state before starting a rollout.

Rollout execution. The worker steps through the environment for the prescribed number of steps. Each particle commits to a single random action, held fixed for the duration of the rollout segment (see [Section 4.4](#)). In the discrete setting, this action is played with probability $1 - \epsilon$ ($\epsilon = 0.2$), with a uniform random action played otherwise. In the continuous setting, the committed action is played deterministically throughout the segment.

Back-reporting. Upon completing the rollout, the worker transmits the endpoint environment checkpoint and cumulative reward back to the coordinator. The coordinator uses these to create a new node in the state-lineage tree ([Section 4.1](#)), which stores only the endpoint checkpoint, cumulative reward, and a parent pointer.

A.3 RND Learner

The uncertainty oracle U is instantiated using standard RND ([Burda et al., 2018](#)), which quantifies novelty via the prediction error of a trained network against a fixed, random target. We choose RND for its scalability and efficiency compared to ensemble-based uncertainty methods ([Osband et al., 2016](#); [Lakshminarayanan et al., 2017](#)). The module consists of a fixed *target network* and a trainable *predictor network*. Both use

standard Atari convolutional torsos (Mnih et al., 2015) followed by MLP heads consisting of two 1024-unit linear layers separated by a ReLU activation. We use orthogonal initialization for the torso weights and normalize inputs (running mean/std) clipped to $[-5, 5]$, consistent with standard RND implementations (Burda et al., 2018). The predictor is trained to minimize the Mean Squared Error (MSE) against the target embedding.

Replay buffer. Workers stream their observations into a shared replay buffer of capacity 512,000. Each entry has the form (s, a) , where s is the observation and a the action.

Asynchronous training. The RND learner continuously samples mini-batches from the shared replay buffer and runs gradient-descent steps to update the predictor network, using a batch size of 128 and Adam with a learning rate of 3×10^{-4} . The coordinator periodically fetches the latest predictor weights from the learner to score particle states.

A.4 Population Management Hyperparameters

Table 5 summarizes the main population management hyperparameters introduced in Section 4.

Table 5: Population management hyperparameters for GOWU. The **MuJoCo** column applies to all continuous-control tasks (AntMaze and Adroit).

PARAMETER	MONTEZUMA	PITFALL	VENTURE	MUJoCo
GROUPS (M)	4	4	4	16
PARTICLES PER GROUP (N)	32	32	32	8
OUTER STEPS RANGE ($[K_{\min}, K_{\max}]$)	[10, 20]	[10, 20]	[6, 16]	[20, 40]
INNER STEPS RANGE ($[T_{\min}, T_{\max}]$)	[5, 15]	[10, 20]	[10, 20]	[3, 4]
ROLLBACK RANGE $[k_{\min}, k_{\max}]$	[1, 3]	[1, 4]	[1, 12]	[1, 20]

A.5 Computational Resources

Table 6 reports wall-clock runtime, exploration score, and the number of RND SGD steps for Phase I of GOWU on *Montezuma’s Revenge*, averaged over 100 seeds. Each run uses the distributed architecture described above with 1 TPU for the RND uncertainty estimator, 128 CPUs (one per rollout worker), and 1 CPU for the coordinator.

Table 6: Computational cost of GOWU Phase I on *Montezuma’s Revenge*, averaged over 100 seeds.

Metric	100M frames	200M frames	300M frames	400M frames
Clock runtime (hours)	4.53 ± 1.84	6.98 ± 1.92	9.01 ± 2.58	10.71 ± 3.35
Mean score	$48,444 \pm 14,417$	$76,014 \pm 16,626$	$89,485 \pm 18,760$	$98,249 \pm 18,102$
RND SGD steps	$0.77\text{M} \pm 0.28\text{M}$	$1.38\text{M} \pm 0.39\text{M}$	$1.86\text{M} \pm 0.57\text{M}$	$2.28\text{M} \pm 0.81\text{M}$

Notably, the total number of RND SGD steps at 400M frames ($\sim 2.3\text{M}$) is comparable to the $\sim 3\text{M}$ model update steps used by intrinsic-motivation baselines such as BYOL-EXPLORE (Guo et al., 2022) and BYOL-HINDSIGHT (Jarrett et al., 2023), indicating no additional computational overhead from the uncertainty estimator relative to standard deep RL training.

B Implementation Details for the Backward Algorithm

Here, we describe our implementation of the backward algorithm. We first explain how demonstrations are decomposed into segments and then detail the curriculum learning strategy applied to each segment. Finally, we provide the specific configuration parameters and hyperparameters used in our experiments.

B.1 Overview and segmentation

Our approach builds on the backward learning algorithm of Salimans and Chen (2018), as also used in the robustification phase of GO-EXPLORE (Ecoffet et al., 2021), and extends it with several modifications. The agent learns to solve the task by starting from states near the end of a demonstration and gradually moving the starting point backwards. To break a single long backward trajectory into smaller, more manageable chunks—making training faster and more stable—we decompose each demonstration trajectory $\tau = \{s_0, a_0, r_0, \dots, s_T\}$ into at most K_{\max} segments delineated by reward events. Concretely, we first identify all timesteps at which the agent receives a non-zero reward. If there are more such timesteps than K_{\max} , we evenly downsample them to obtain exactly K_{\max} boundary points. Let T_k denote the k -th selected boundary; segment k then covers the portion of the trajectory culminating at T_k . For Atari, we set $K_{\max} = 10$; for the MuJoCo tasks (Adroit and AntMaze), we set $K_{\max} = 1$, treating the entire demonstration as a single segment where the starting state is progressively moved back toward the initial state. Our implementation supports training on multiple demonstrations simultaneously: each demonstration is segmented independently. Importantly, the resulting segments are not simply aggregated into a flat pool; the system tracks the ordering of segments and which demonstration each segment originates from, since each segment’s curriculum window is allowed to extend backward beyond the segment’s own start boundary.

Distributed architecture. The system uses a distributed actor-learner architecture. A centralized *curriculum server* maintains the global curriculum state—tracking the current start index, and success rates for every segment—and serves starting states to the actors. Multiple distributed *actors* concurrently fetch start states from the curriculum server, execute episodes, and stream trajectories to a centralized *learner*, which continuously updates the PPO policy weights. Background *evaluators* run asynchronously, periodically fetching the latest weights to assess performance (see Section B.6). This architecture allows the algorithm to learn different stages of the task in parallel, scaling efficiently with the number of actors.

B.2 Curriculum strategy

For a chosen segment ending at T_{end} , the curriculum maintains a *current start index* t_{curr} (initially set to T_{end}) and a fixed window size Δ . This index represents the latest point in the trajectory from which the agent is currently learning to reach the segment’s goal. The curriculum dynamically adjusts the start position based on the agent’s performance.

State sampling. At the beginning of an episode, a start index t_{start} is sampled uniformly from the interval $[t_{\text{curr}} - \Delta, t_{\text{curr}}]$. The environment is reset to the state $s_{t_{\text{start}}}$ from the demonstration.

Success criteria. An episode is considered successful if the agent achieves a return R_{agent} comparable to the return of the demonstration segment from t_{start} to T_{end} , denoted as $R_{\text{demo}}(t_{\text{start}})$. Success is strictly defined as:

$$R_{\text{agent}} \geq R_{\text{demo}}(t_{\text{start}}) - \varepsilon_{\text{tol}}$$

where ε_{tol} is a tolerance parameter (see Table 8 for environment-specific values). An episode is terminated early if the number of steps exceeds $\mu \cdot \bar{L} + b$, where \bar{L} is an exponential moving average (with smoothing factor $\alpha = 0.9$) of successful rollout lengths, $\mu = 2.0$ is a multiplier, and b is a fixed buffer ($b = 500$ by default; $b = 100$ for Adroit). For Atari, training episodes are additionally terminated early upon loss of life; for AntMaze, episodes are terminated if the ant flips over (see Appendix F).

Curriculum progression. The curriculum tracks the success rate S over a buffer of the most recent N_{update} rollouts. Two distinct success thresholds govern progression:

- **Regression (moving backwards):** If $S \geq S_{\text{req}}$ (default 0.2), the window moves backward to include earlier states. The current start index is updated as $t_{\text{curr}} \leftarrow \max(0, t_{\text{curr}} - \delta_{\text{back}})$, where the step size δ_{back} is sampled uniformly from $[\alpha_{\text{dec}} \cdot \Delta, \beta_{\text{dec}} \cdot \Delta]$. Here, α_{dec} and β_{dec} are decrease multipliers that control the step size range (see Table 8). This stochastic step size prevents the curriculum from getting stuck in local cycles. Note that the lower bound is the absolute beginning of the demonstration (the initial state), not the beginning of the segment; this means the curriculum window for a given segment can extend well beyond the segment’s own start boundary, and each segment’s curriculum eventually requires the agent to achieve the segment’s reward target starting from the very beginning of the demonstration.

- **Simplification (moving forwards):** If $S < S_{\text{req}}$, the task is deemed too difficult, and the window moves forward. The update is $t_{\text{curr}} \leftarrow \min(T_{\text{end}}, t_{\text{curr}} + \delta_{\text{fwd}})$, where the step size δ_{fwd} is sampled uniformly from $[\alpha_{\text{inc}} \cdot \Delta, \beta_{\text{inc}} \cdot \Delta]$, with α_{inc} and β_{inc} being the increase multipliers.
- **Completion criterion:** When t_{curr} reaches step 0 (the beginning of the demonstration), a stricter threshold $S_{\text{req,begin}} = 0.95$ must be met before the segment is considered solved. This ensures the agent can reliably execute the full trajectory from the very start of the demonstration to the segment’s reward boundary.

B.3 Environment-specific configurations

The backward curriculum is configured differently across environment families:

Atari (Montezuma’s Revenge, Pitfall!, Venture). Demonstrations are decomposed into up to $K_{\text{max}} = 10$ segments. The window size is $\Delta = 25$, and the decrease/increase multipliers are $(\alpha_{\text{dec}}, \beta_{\text{dec}}) = (0.25, 0.75)$ and $(\alpha_{\text{inc}}, \beta_{\text{inc}}) = (0.5, 1.0)$, respectively. For *Montezuma’s Revenge* and *Venture*, reward clipping is applied (bounding cumulative targets to $[-1, 1]$) with a strict tolerance $\epsilon_{\text{tol}} = 0$. For *Pitfall!*, rewards are scaled by 0.001 (without clipping) and the tolerance is relaxed to $\epsilon_{\text{tol}} = 1500$ to accommodate the game’s scoring structure, where the agent can lose points. For *Montezuma’s Revenge*, the agent’s observations include the frame at which the last reward was received, providing context when the same room appears multiple times in a demonstration. Additionally, after successfully achieving the segment’s reward target, the agent is allowed to continue playing for a random number of extra frames (up to $\sim e^7 \approx 1096$); this provides additional exploration beyond the target state.

Adroit (door, hammer, relocate). The entire demonstration is treated as a single segment ($K_{\text{max}} = 1$). The window size is reduced to $\Delta = 3$, and all multipliers are set deterministically to $1/3$, removing the stochastic step-size variation. Intermediate contact rewards from Phase I are discarded; only task-completion events are used as reward signals. During the backward curriculum, the goal configuration (i.e., the randomized target location and object placement) is held fixed to the one used during exploration. Whenever an actor samples a start index of 0 from the curriculum window, the episode uses a clean environment reset (i.e., a true `env.reset()`, which randomizes the goal configuration). This allows the policy to begin generalizing across target locations and object placements.

AntMaze. As with Adroit, the demonstration is treated as a single segment ($K_{\text{max}} = 1$). The window size is $\Delta = 25$. An action repeat of 4 is applied. Clean environment resets are used whenever an actor samples a start index of 0, as described above for Adroit. The PPO batch size is reduced from 128 to 64 (this is mainly to avoid out-of-memory errors).

B.4 Agent architecture

We use Proximal Policy Optimization (PPO) as the underlying reinforcement learning algorithm. The policy and value functions use separate encoders based on the IMPALA ResNet architecture (Espenholt et al., 2018), each followed by fully connected layers. For Atari, each encoder feeds into a dense layer of size 1024, followed by policy and value heads of size 512. For Adroit and AntMaze, the architecture is scaled down (to avoid out-of-memory errors): the dense layer is 512, and the policy and value heads are 256 each. The encoder input varies by environment; see Appendix E for details on the observation processing pipeline for each environment family.

B.5 Hyperparameters and configuration

For each demonstration, we run on 5 random seeds.

Consistent with GO-EXPLORE, we use reward clipping on *Montezuma’s Revenge* and *Venture*, and reward scaling on *Pitfall!*.

Table 7: PPO Hyperparameters (defaults; see Section B.3 for environment-specific overrides).

Parameter	Value
Optimizer	Adam
Learning Rate	1×10^{-4}
Discount Factor (γ)	0.999
GAE Lambda (λ)	0.95
Unroll Length	128
Batch Size	128 (64 for AntMaze)
Num Epochs	1
Num Minibatches	8
Entropy Cost	1×10^{-3}
Value Cost	0.5
PPO Clipping (ϵ)	0.1
Max Gradient Norm	0.5
Shared Dense Layer	1024 (512 for Adroit/AntMaze)
Policy/Value Head	512 (256 for Adroit/AntMaze)

Table 8: Backward Algorithm Configuration (defaults; see Section B.3 for environment-specific overrides).

Parameter	Value
Required Success Rate (S_{req})	0.2
Completion Threshold ($S_{\text{req,begin}}$)	0.95
Start delta window (Δ)	25 (3 for Adroit)
Min Rollouts for Update (N_{update})	32
Decrease Multipliers ($\alpha_{\text{dec}}, \beta_{\text{dec}}$)	0.25, 0.75 ($\frac{1}{3}, \frac{1}{3}$ for Adroit)
Increase Multipliers ($\alpha_{\text{inc}}, \beta_{\text{inc}}$)	0.5, 1.0 ($\frac{1}{3}, \frac{1}{3}$ for Adroit)
Failure Reward Tolerance (ϵ_{tol})	0 (1500 for Pitfall)
EMA Smoothing Factor (α)	0.9
Early Termination Multiplier (μ)	2.0
Rollout Length Buffer (b)	500 (100 for Adroit)

B.6 Evaluation

A background evaluator runs concurrently with training: it periodically fetches the latest policy weights from the learner and executes evaluation rollouts using the deterministic (mode) version of the policy. During training, we run 10 rollouts per evaluation for Atari and 30 for MuJoCo, and track the best-performing checkpoint based on these periodic evaluations.

Training budget. For Atari, we train for 15–20B environment frames. For MuJoCo, training continues until all segments have been solved with the 95% completion threshold ($S_{\text{req,begin}}$). Table 9 reports the total number of environment frames consumed during Phase II for each MuJoCo task, across 10 runs.

Final evaluation. After training is complete, we perform a dedicated evaluation of the best checkpoint identified during training. This checkpoint is evaluated on 500 rollouts to produce the final policy score.

Evaluation heuristics. A well-known exploit in *Montezuma’s Revenge* allows the agent to remain in a treasure room and collect 1,000-point rewards indefinitely by repeating a specific action sequence, without progressing to the next level. To prevent this from inflating evaluation scores, the evaluator monitors for consecutive rewards of exactly 1,000 points. If 30 or more such consecutive rewards are detected, the rollout is immediately discarded.

Table 9: MuJoCo Phase II training budget: total environment frames consumed per task, across 10 runs (each averaged over 5 seeds).

TASK	MEDIAN	STD	MAX
HAMMER	9,876,809	2,340,952	19,878,384
DOOR	27,629,359	14,928,478	54,589,532
RELOCATE	221,653,220	146,455,143	827,483,942
ANTMAZE	119,160,557	84,845,527	667,819,039

C Environment Checkpointing

Both Phase I and Phase II rely on environment resets to restore particles or training episodes to previously visited states. Reconstructing the environment mid-trajectory requires checkpointing both the simulator’s physical state and the agent’s observation history (e.g., frame stacks). The mechanism differs across environment families:

- **Atari:** We extract and restore the internal ALE emulator state along with the frame stacker’s observation history, following the implementation of Yin et al. (2023, Page 21).
- **Adroit:** We checkpoint the MuJoCo physics state (joint positions and velocities), the random seed (which determines the randomized object and target positions), and task-specific state variables (e.g., whether contact with the target surface has been established).
- **AntMaze:** In addition to the MuJoCo physics state, we save the random seed (which determines the randomized goal coordinates) and the pixel observation stack from the third-person camera renders.

In all cases, the frame stack is replaced with the one saved at checkpoint time.

D Pitfall Timer

Unlike *Montezuma’s Revenge* and *Venture*, *Pitfall!* includes a twenty-minute termination timer. We disable this timer during Phase I to allow non-episodic exploration with GOWU, but final policies are evaluated with the standard timer active. Concretely, we reset the timer at each step by directly writing to the Atari emulator’s RAM via `ale.setRAM()`. The timer is encoded across two RAM bytes: byte 88 stores the minutes and byte 89 stores the seconds. Because the game uses a non-standard internal encoding, we maintain hardcoded lookup tables that map standard minute and second values to the corresponding RAM integers expected by the emulator. We avoid setting the timer to exactly 20:00 or 0:00, as both boundary values trigger unintended side effects in the game state; in practice, we reset it to 19:59. This timer reset is applied only during Phase I exploration and is disabled during Phase II and evaluation.

E Observation Processing

This section describes the observation processing pipeline for each environment family. All pipelines produce grayscale, frame-stacked tensors normalized to $[0, 1]$; the specifics differ per domain and are detailed below.

E.1 Atari

For the Atari environments, we build on the standard DeepMind ACME preprocessing wrappers. The environment is initialized using the `NoFrameskip` variant (or `v0` with sticky actions) to obtain raw 60 Hz frames with the full 18-action space exposed.

Temporal pooling and grayscaling. After each action repeat of 4 frames, temporal max-pooling is applied element-wise over the last 2 of the 4 frames to prevent sprite flickering artifacts. The resulting RGB image is converted to grayscale via the standard luminosity formula $Y = 0.299R + 0.587G + 0.114B$.

Downsampling. The grayscale image is resized to the target resolution of 84×84 pixels. Two variants are used:

- *Standard (Montezuma, Pitfall):* The grayscale frame (210×160) is directly resized to 84×84 using bilinear interpolation.
- *With spatial max-pooling (Venture):* A 2×2 spatial max-pooling step is applied first to preserve small, bright sprites (e.g., the player dot) that would otherwise be smoothed out by bilinear interpolation. This reduces the resolution to 105×80 , which is then resized to 84×84 via bilinear interpolation.

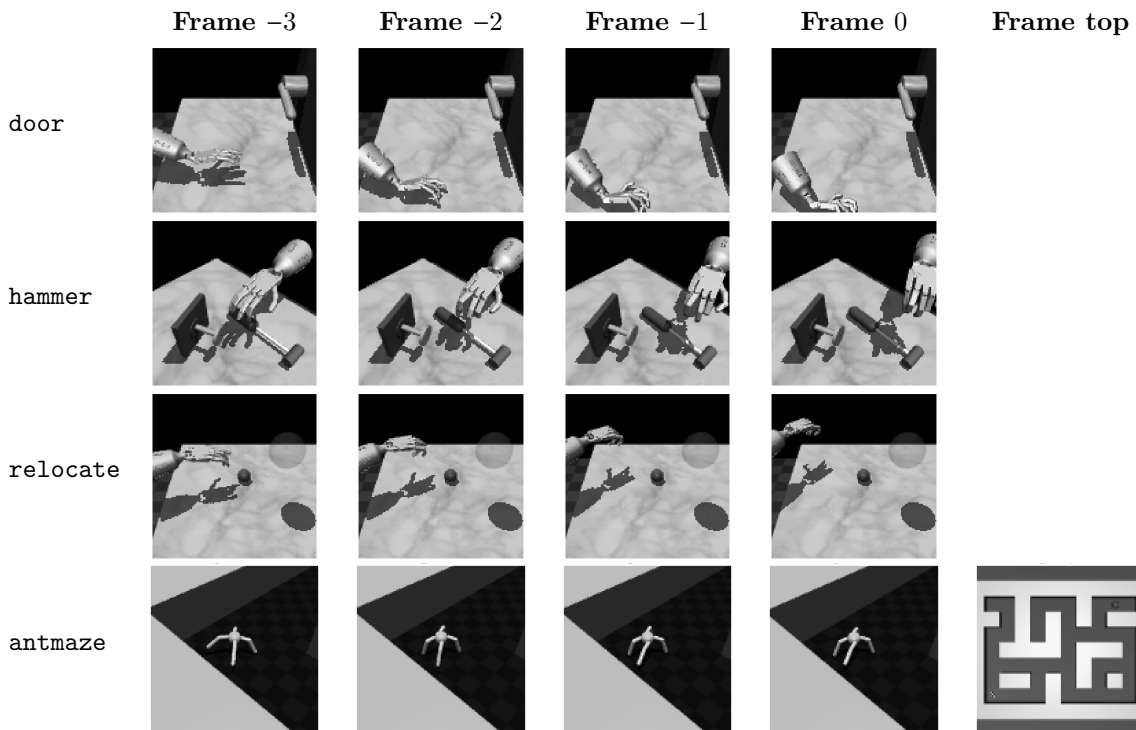


Figure 6: Processed visual observations as seen by the agent for each MuJoCo task. Each column shows a frame in the observation stack, from the oldest (Frame -3) to the most recent (Frame 0). For AntMaze, the “Frame top” column shows the global top-down view of the maze; during Phase I (exploration), only this top-down view is used. See Section 5 for an overview and Appendix E for full details on the observation processing pipeline.

Normalization and frame stacking. Pixel values are cast to floating-point and scaled to $[0, 1]$. The 4 most recent processed frames are stacked along the channel axis, producing a final observation tensor of shape $84 \times 84 \times 4$. For Phase II (backward learning) on *Montezuma’s Revenge*, a fifth frame is appended corresponding to the most recent reward observation—i.e., the frame at which the agent last received a reward (see Appendix B for details).

E.2 Adroit

Pixel rendering. Rather than using the standard gym rendering interface, we attach a `mujoco.MovableCamera` to the physics state and render directly at 120×120 pixels in RGB. For each task, the camera pose is locked to a fixed, task-specific viewpoint:

- `hammer-v0`: Lookat = $[0, -0.15, 0.15]$, Distance = 0.7, Azimuth = -45° , Elevation = -45° .
- `door-v0`: Lookat = $[0, -0.1, 0.25]$, Distance = 0.8, Azimuth = 60° , Elevation = -35° .
- `relocate-v0`: Lookat = $[0, -0.1, 0.15]$, Distance = 0.9, Azimuth = -180° , Elevation = -45° .

Grayscaleing, normalization, and frame stacking. The rendered RGB image is converted to grayscale

via the luminosity formula. Four consecutive frames are stacked along the channel axis, producing a tensor of shape $120 \times 120 \times 4$. Pixel values are normalized to $[0, 1]$.

E.3 AntMaze

Scene modification. To make the task visually solvable, the environment scene is dynamically modified: a semi-transparent red sphere is injected at the goal coordinates via a scene callback, and the floor color is set to dark gray $([0.2, 0.2, 0.2])$ for improved contrast when textures are disabled.

Dual camera rendering. Two views are rendered at 120×120 pixels using a `mujoco.MovableCamera`:

- *Global top-down view:* Locked high above the maze center (Lookat = $[18, 12, 0]$, Distance = 55, Azimuth = 90° , Elevation = -90°). Textures are disabled to provide a clean structural map of the maze layout and goal marker.
- *Third-person egocentric view:* Dynamically tracks the agent’s position (Distance = 8, Azimuth = 135° , Elevation = -45°) with textures enabled for rich visual feedback of the ant’s limbs and surroundings.

Both views are converted to grayscale and resized to 120×120 using Lanczos resampling.

Frame stacking variants. During Phase I (exploration), only the global top-down view is used, yielding an observation of shape $120 \times 120 \times 1$. During Phase II (policy distillation), the global frame is stacked with 4 historical egocentric frames, producing an observation of shape $120 \times 120 \times 5$ (channel 0: global map; channels 1–4: temporal egocentric history). Pixel values are normalized to $[0, 1]$.

F MuJoCo Reward and Dead-State Extraction

This appendix details the sparse reward and dead-state detection logic used during Phase I exploration for the MuJoCo environments.

F.1 AntMaze: Flip Detection

If the ant flips over, it cannot recover, rendering the remainder of the episode useless. We detect flips using two quantities extracted from the MuJoCo physics state at every step:

1. *Z-coordinate* (z): the absolute height of the ant torso, retrieved via `physics.data.qpos[2]`.
2. *Upward vector* (z_{up}): the (2, 2) element of the torso’s 3×3 orientation rotation matrix

`physics.data.xmat[torso_id],`

representing the Z-component of the torso’s local “up” vector in the world frame.

The ant is flagged as flipped if either $z < 0.2$ (torso near the ground) or $z_{\text{up}} < 0$ (torso upside-down). Upon detection, the particle is assigned a DEAD state. If the agent triggers `goal_achieved` on the same step as a flip, the particle is still marked as DEAD.

F.2 Adroit: Sparse Contact Rewards

For all Adroit tasks, the standard continuous rewards are replaced by a sparse reward wrapper that parses the MuJoCo contact information at every step. Contact is evaluated by extracting geometry (geom) IDs from the model and iterating through active collisions in `physics.data.contact`, using explicit geom whitelists to prevent false positives (e.g., the hand contacting the table rather than the target object). If the underlying environment flags `goal_achieved = True`, the agent receives a +1 terminal reward. The task-specific logic is:

- **hammer-v0:** Contact is checked between the 19 geoms comprising the robot hand (wrist, palm, and finger joints) and the hammer object. A reward of +1 is assigned when the hand first contacts the hammer. If contact is subsequently lost, the particle is marked as DEAD.

- **door-v0**: Contact is checked between the hand geoms and the door latch/handle geoms. A reward of +1 is assigned upon first contact. Loss of contact triggers a DEAD state.
- **relocate-v0**: Contact is checked between the ball and all geoms *except* a whitelist of forbidden surfaces (floor and table geoms). A reward of +1 is assigned when any hand surface first contacts the ball. If contact with the ball is subsequently lost, the particle is marked as DEAD.

G Ablation Study

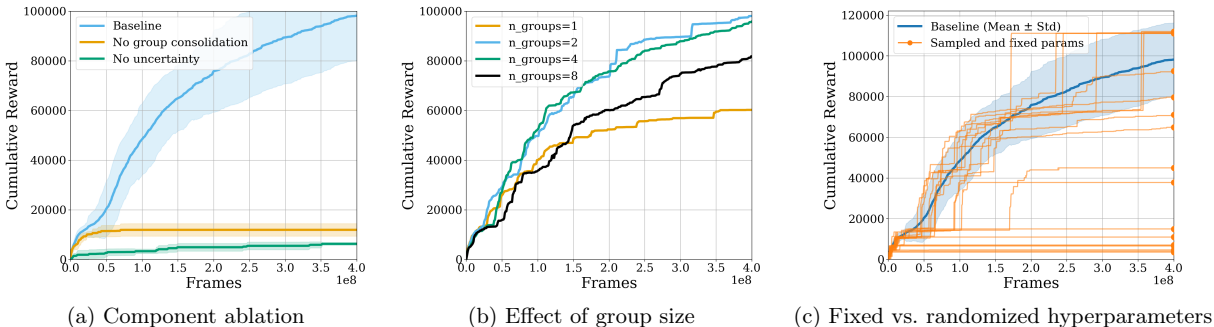


Figure 7: Ablation studies on *Montezuma’s Revenge*. Mean cumulative reward (\pm std) across seeds. (a) Disabling uncertainty-based winner selection causes exploration to fail; disabling group consolidation degrades performance. (b) 2 and 4 groups perform similarly; 1 group is worst; 8 groups improve over 1 but underperform 2 and 4. (c) Per-iteration hyperparameter randomization yields robust performance without tuning.

To validate the design choices underlying GOWU, we conduct a series of ablation experiments on *Montezuma’s Revenge*. Unless stated otherwise, we report the mean cumulative reward (with standard deviation) along the exploration path as a function of game frames.

All ablations are conducted on *Montezuma’s Revenge* with 8 seeds per variant (the baseline uses 100 seeds; see Section 5.1). Figure 7 presents the results across three experiments.

Component ablation. We disable individual components of GOWU while keeping everything else fixed (Figure 7a). Removing the uncertainty estimator (selecting the winner uniformly at random among surviving particles instead) causes exploration to fail; the variant does not complete the first level. This confirms that epistemic uncertainty is critical for directing the search toward under-explored regions. Disabling the group consolidation step (Algorithm 1, Line 30) also degrades performance, though the variant still does slightly better than the no-uncertainty ablation. This indicates that periodically collapsing the population to the group’s most uncertain state accelerates progress. An additional benefit of group consolidation is that it results in more frequent pruning, keeping the lineage tree smaller and reducing memory usage.

Effect of group size. We vary the number of parallel groups $M \in \{1, 2, 4, 8\}$ while keeping the total number of particles fixed at 128 (i.e., $N = 128/M$ per group) (Figure 7b). Using $M = 2$ and $M = 4$ groups yields similar performance; $M = 1$ (a single group) is the worst, and $M = 8$ improves over $M = 1$ but underperforms $M \in \{2, 4\}$, because the number of particles per group drops to 16, making it harder to leverage the particle management logic (winner selection, pruning, and rollback) to navigate around obstacles.

Robustness to hyperparameter randomization. In our standard configuration, the population management hyperparameters (K , T , and rollback depth) are sampled uniformly from their respective ranges at each iteration. To test robustness, we run an alternative protocol with 20 seeds in which a single draw from each range is fixed for the entire run; different seeds thus correspond to different fixed hyperparameter settings (Figure 7c). Per-iteration randomization yields consistently strong performance, whereas the fixed-draw protocol produces high variance across seeds. This demonstrates that randomization provides inherent robustness: sampling from a reasonable range at each step is sufficient, without needing to identify a single optimal setting.

H Additional Related Works

Evolutionary and population-based methods. GowU’s population-based nature connects it to evolutionary methods, which drive exploration by evolving diverse populations of policies. Foundational approaches such as Novelty Search, MAP-Elites, and the quality-diversity literature reward behavioral novelty or coverage (Lehman and Stanley, 2011; Mouret and Clune, 2015; Pugh et al., 2016). More recent hybrids combine such diversity mechanisms with deep RL and policy-gradient updates (Conti et al., 2018; Parker-Holder et al., 2020; Wang et al., 2025). Although both families maintain populations, their mechanisms for driving exploration differ fundamentally: unlike GowU, which searches directly in state space, these methods operate in the parameter space of a policy, generating diversity by perturbing model weights.

Additional differences between GowU and MCTS. GowU and MCTS also differ in how search is guided and in the kinds of action spaces they most naturally accommodate. Standard MCTS is usually guided by value estimates or visit counts, whereas GowU uses epistemic uncertainty as a primary signal for redistributing exploration effort. Recent work on Epistemic MCTS augments MCTS with epistemic uncertainty for deeper exploration (Oren et al., 2022), but remains a non-particle-based search method. In addition, standard MCTS most naturally fits discrete action spaces, while continuous-action variants typically require extra machinery such as progressive widening (Couëtoux et al., 2011). GowU does not enumerate actions at tree nodes in this way: particles can execute rollouts using arbitrary policies, which allows the framework to accommodate continuous actions more directly.

Latent Go-Explore. Latent Go-Explore (Gallouédec and Dellandréa, 2023) addresses the reliance of Go-Explore on hand-designed observation discretization by replacing it with a learned latent representation. However, learning such a representation itself requires sufficiently rich exploration data, creating a potential chicken-and-egg issue. Moreover, the method is evaluated only in terms of exploration performance, where it slightly improves over Go-Explore on *Montezuma’s Revenge* and *Pitfall!*. It remains unclear whether this cell-free variant also supports the subsequent policy-learning stage needed to obtain a deployable policy.

MuJoCo baselines. For the MuJoCo tasks evaluated in this work, direct baselines are unavailable.

For Adroit, recent visual RL methods such as DRM (Xu et al., 2023) and MENTOR (Huang et al., 2025) solve `door` and `hammer` from pixels without demonstrations, but rely on dense reward shaping. With privileged state observations, Wang and Zhao (2024) solve `door` and `hammer` using sparse rewards and model-based intrinsic motivation, but do not use pixels. To the best of our knowledge, no existing method solves these tasks from *pixel observations* in the sparse-reward setting without expert demonstrations or offline datasets. The `relocate` task, in particular, remains unsolved from pixels even with dense rewards; with state observations, it has been solved using dense reward shaping (Rajeswaran et al., 2017). We note that our Phase I exploration does augment the sparse environment reward with a single intermediate reward signal and a dead-state condition, both derived from privileged state information (see Appendix F for details); these are far simpler than the dense reward shaping required by standard RL methods, but they do go beyond a purely sparse reward signal.

For AntMaze, DIRECTOR (Hafner et al., 2022) solves an egocentric ant maze from first-person pixel inputs with sparse rewards, but their custom maze is smaller than ours (`antmaze-large-diverse-v0`) and uses uniquely colored walls as navigation landmarks. Several goal-conditioned RL methods (Bortkiewicz et al., 2024; Kim et al., 2021) achieve moderate success rates on AntMaze benchmarks using the JaxGCRL framework (e.g., ~65% on AntMaze-large), but operate from state observations with fixed start and goal locations. In contrast, our setup learns entirely from images with randomized goal locations. We note, however, that our training uses the default environment randomization, where the target location is slightly perturbed around a fixed point across seeds. This differs from the D4RL-style “diverse” setting (Fu et al., 2020), where trajectories span substantially different start and goal configurations, requiring greater generalization.

Resets and simulation in RL. Resets are sometimes viewed as infeasible for physical robots (Eysenbach et al., 2017; Gupta et al., 2021), but this view overlooks the central role of simulation in modern AI training. Even for physical applications, policies are increasingly pre-trained in simulation—from robotic manipulation to autonomous driving (Qassem et al., 2010; Bojarski et al., 2016; Tobin et al., 2017; Akkaya et al., 2019; Bansal et al., 2018)—making resets a readily available primitive. The empirical success of planning algorithms

such as AlphaZero (Silver et al., 2016, 2018) provides further evidence for the power of reset-based search.

Temporal contrastive features for exploration. Temporal contrastive features (Myers et al., 2024; Mohamed et al., 2026; Liu et al., 2024) learn representations that capture the temporal structure of the environment, offering a potentially stronger basis for planning-aware and noise-robust exploration than prediction-error-based methods such as RND.

I *Montezuma’s Revenge* Middle Room Bug

During exploration, we discovered a previously undocumented bug in *Montezuma’s Revenge* that occurs in the *middle room* of each level (the room containing a torch and a rolling skull). Figure 8 illustrates the bug sequence frame by frame: the agent, positioned on the rope on the right-hand side of the room (Frame -4), jumps to the left and progressively approaches the platform where the rolling skull patrols (Frames -3 through -1), eventually making contact with the platform (Frame 0). If the agent is carrying a key at the time of contact, the key is consumed and a reward is collected. Since the key in the first room respawns periodically after a sufficient delay (Salimans and Chen, 2018), the agent can return, re-acquire it, and repeat the process indefinitely, creating an infinite reward loop that traps the agent in the same level and prevents further exploration.

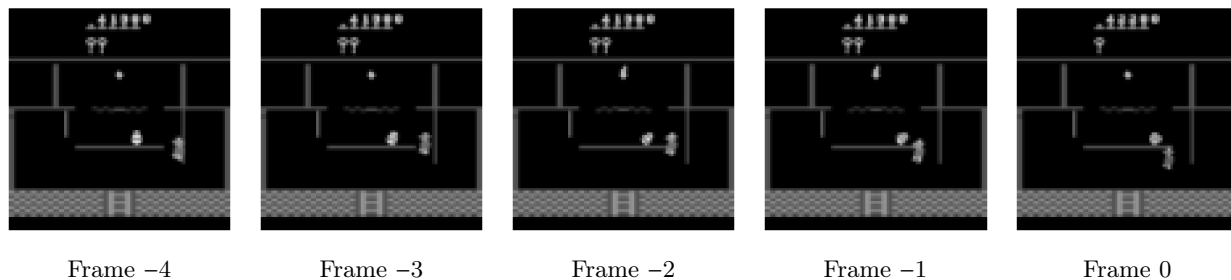


Figure 8: Frame-by-frame illustration of the middle room bug in *Montezuma’s Revenge*. The agent starts on the rope (Frame -4), jumps left, and hits the skull platform (Frame 0), losing a key and collecting an unintended reward.

To prevent the algorithm from exploiting this glitch, we employ a two-step visual detection heuristic that activates whenever a positive reward is registered.

Step 1: Location verification. We first determine whether the agent is currently in the middle room. A fixed 20×20 spatial crop of the current frame is extracted from a region that uniquely identifies this room. The crop is compared against a pre-recorded set of reference crops from the middle room across different game levels using the L2 norm (Euclidean distance). If the pixel-wise distance is below a small threshold, the agent is confirmed to be in the middle room.

Step 2: Action verification. If the location check passes, we verify whether the agent has just performed the bugged action (jumping off the rope). We inspect the agent’s last four frames (as shown in Figure 8) and isolate a bounding box covering the area where the rope sequence takes place. The maximum pixel-wise difference between consecutive frames in this region is computed; if it exceeds a threshold, it indicates a sudden burst of movement consistent with the visual signature of the agent jumping off the rope.

Intervention. If a positive reward is received while *both* visual conditions are simultaneously satisfied, the reward is flagged as an exploit and the particle is immediately marked as DEAD. This ensures the buggy particle will never be selected as a winner; instead, at the next GOWU redistribution step, it will be replaced by a clone of the current winner—a non-buggy particle—and exploration resumes from a valid state.

J *Montezuma’s Revenge* Key Respawn Mechanism

In *Montezuma’s Revenge*, the key in the first room respawns after a sufficient amount of time has elapsed, a feature previously documented by Salimans and Chen (2018). Some of our highest-scoring distilled policies exploit this mechanism: rather than traveling to distant rooms to collect keys, they learn to move back and forth between the first room and an adjacent room, waiting for the key to reappear. By collecting keys without traversing the full level, the agent can sometimes complete levels faster, leading to the especially high scores observed for the best Phase II runs. We note that this is a feature of the game, not a bug; in fact, waiting for the key to respawn is sometimes necessary, as certain levels require the first room’s key multiple times to advance.

K Why GWTW is Exponentially Faster: A Concrete Example

Consider the problem of finding the deepest node in an unknown tree. DFS and BFS may, in the worst case, need to visit every node before reaching it. GWTW takes a different approach: it advances a population of particles in parallel, kills those that reach leaves, and clones survivors to maintain the population size. This pruning-and-cloning mechanism redirects all computational effort toward branches that remain alive. We illustrate this with a concrete tree where DFS and BFS both require $\Theta(2^D)$ node evaluations to find the unique deepest node, while GWTW succeeds with only $\mathcal{O}(D \log(D/\delta))$.

Tree construction. Let D be a depth parameter. We construct a tree T with a unique deepest node at depth $D + 1$:

- **Spine (golden path):** Nodes v_0 (root), v_1, \dots, v_{D+1} . Each spine node v_i ($0 \leq i \leq D - 1$) has exactly two children: v_{i+1} and a trap root t_i . Node v_D has a single child v_{D+1} , which is a leaf and the unique deepest node.
- **Trap subtrees:** Each t_i roots a subtree where every internal node has 6 children: 2 internal nodes and 4 leaves (immediate dead ends). Trap subtrees extend down to depth $D - 1$, at which point all 6 children are leaves (at depth D).

Because each trap node spawns 2 internal children, the traps grow like binary trees. The total number of nodes in T is $\Theta(2^D)$.

Inefficiency of DFS and BFS. Both algorithms must process the full tree volume:

- **BFS** explores layer by layer. To reach depth $D + 1$, it must visit all $\Theta(2^D)$ nodes at preceding levels. **Cost:** $\Theta(2^D)$.
- **DFS** (randomized) has a $1/2$ probability of entering a trap at each spine node. Since the earliest traps contain $\Theta(2^D)$ nodes that must be exhaustively explored before backtracking, even a single wrong turn is catastrophic. **Cost:** $\Theta(2^D)$.

Note that independent random walks also fail: reaching v_{D+1} requires taking the correct branch D times in a row, which happens with probability 2^{-D} .

Analysis of GWTW. GWTW maintains B particles, all starting at v_0 . At each step: (1) every particle moves to a uniformly random child; (2) particles landing on leaves die; (3) survivors are resampled with replacement to restore the population to B .

Let x_i denote the expected fraction of particles at spine node v_i . When particles at v_i step forward, both children (v_{i+1} and t_i) are non-leaves, so all golden-path particles survive: $x_i/2$ land on v_{i+1} and $x_i/2$ enter the trap. Meanwhile, trap particles each choose among 6 children (2 internal, 4 leaves), surviving with probability $1/3$. The total survivor fraction is:

$$S_i = \underbrace{x_i}_{\text{golden survivors}} + \underbrace{\frac{1 - x_i}{3}}_{\text{trap survivors}} = \frac{1 + 2x_i}{3}. \quad (1)$$

After resampling, the fraction on the golden path becomes:

$$x_{i+1} = \frac{x_i/2}{S_i} = \frac{3x_i}{2(1+2x_i)}. \quad (2)$$

Starting from $x_0 = 1$, this recurrence produces: $1 \rightarrow 1/2 \rightarrow 3/8 \rightarrow 9/28 \rightarrow \dots$, converging monotonically from above to the fixed point $x^* = 1/4$. Since the map $f(x) = \frac{3x}{2+4x}$ is strictly increasing with $f(1/4) = 1/4$, the sequence remains above $1/4$ for all i . This is the key insight: because traps kill particles at rate $2/3$ per step while the golden path kills none, GWTW automatically maintains at least 25% of its population on the correct path, regardless of the exponential volume of the traps.

Cost of GWTW. At each depth, the expected number of golden-path particles is at least $B/4$. By a Chernoff bound, the probability that this count drops to zero at any single depth is at most $\exp(-cB)$ for a constant $c > 0$. Applying a union bound over D levels, the probability that GWTW ever loses the golden path is at most $D \cdot \exp(-cB) \leq \delta$ whenever $B \geq \frac{1}{c} \ln\left(\frac{D}{\delta}\right)$. The total number of node evaluations is therefore:

$$\text{Cost}_{\text{GWTW}} = \mathcal{O}(B \cdot D) = \mathcal{O}\left(D \log \frac{D}{\delta}\right), \quad (3)$$

which is exponentially smaller than the $\Theta(2^D)$ cost of DFS and BFS. Note that for any fixed search strategy, adversarial trees can be constructed that force $\Omega(2^D)$ work. The fundamental reason GWTW succeeds is that parallel exploration with redistribution amplifies the probability of advancing at each depth level: in the example above, at each level GWTW only requires *at least one* of B particles to follow the spine rather than enter a trap, after which cloning restores the population to B for the next level. A single walker, by contrast, must choose the spine over a trap at all D levels in sequence, succeeding with probability 2^{-D} . GWTW converts this multiplicative success probability into an additive failure probability of $D \cdot e^{-cB}$ for a constant $c > 0$.